Laser-based primary thermometry: a review

R. Gotti[1a], M. Lamperti[1], D. Gatti[1] and M. Marangoni[1a]

AFFILIATIONS

[1]*Dipartimento di Fisica - Politecnico di Milano and IFN-CNR, Via Gaetano Previati 1/C, 23900 Lecco, Italy*

[a)]**Authors to whom correspondence should be addressed:** *riccardo.gotti@polimi.it, marco.marangoni@polimi.it*

Keywords: Absolute Primary Thermometry, Doppler broadening Thermometry, Precision Molecular Spectroscopy

ABSTRACT

Laser-based primary thermometry was initiated almost 15 years ago by the proposal to determine the absolute temperature of a gas at thermodynamic equilibrium through the Doppler width of an associated absorption transition, exploiting the potentially very accurate measurement of an optical frequency to infer the elusive thermal energy of a molecular or atomic absorber. This approach, commonly referred to as Doppler broadening thermometry, has benefited across the years from substantial improvements, of both technical and fundamental nature, eventually reaching an accuracy of about 10 ppm on the temperature determination in the best cases. This is sufficient for Doppler broadening thermometry to play a significant role in the practical realization of the new kelvin, which follows the 2019's redefinition from a fixed value of the Boltzmann constant, and to tackle the challenge, among others, to quantify and possibly fix systematic uncertainties of the international ITS-90 temperature scale. This paper reviews and comparatively analyses methods and results achieved so far in the field of laser-based primary thermometry, also including spectroscopic approaches that leverage the temperature-dependent distribution of line intensities and related absorbances across the ro-vibrational band of a molecular sample. Although at an early stage of development, these approaches show a promising degree of robustness with respect to the choice of the line-shape model adopted for the fitting of the absorption spectra, which is a delicate aspect for all laser-based thermometers. We conclude identifying possible technical and scientific evolution axes of the current scenario.

1. Introduction

1.1. The *Mise en pratique* of the new kelvin and the ITS-90 temperature scale

On November 16th 2018 the *Conférence générale des poids et mesures* (CGPM) approved the revision of the International System of Units (SI), shifting the definition of SI units from a particular property of matter of a primary sample to a direct link with a fundamental constant. Such paradigmatic shift affected the definition of the ampere, the kilogram, the mole and the kelvin starting from May 20th 2019.

As highlighted in Fig.1 the kelvin, the SI unit for the absolute temperature, has been redefined in terms of a fixed value of the Boltzmann constant $k_{\mathrm{B}} = 1.380649 \times 10^{-23}\ \mathrm{JK}^{-1}$[1], rather than as a fraction of the temperature of the triple point of water (TPW). Since then, every physical system at TPW that was previously used to determine k_{B} from an indirect measurement of the microscopic thermal energy $(k_{\mathrm{B}}T)$, can now be exploited as an absolute primary thermometer for the so-called *Mise en pratique* of the kelvin (MeP-K)[2-5]. The purpose of MeP-K is to provide approaches and methodologies to determine the thermodynamic temperature in an absolute way.

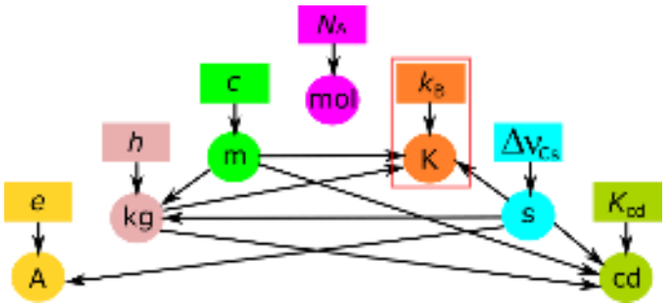

Figure 1 Schematic diagram of the links between SI units and physical constants according to the 2019 redefinition. The fixed constants (rectangles) are the electron charge (e), the Planck constant (h), the speed of light (c), the Avogadro number (N_A), the Boltzmann constant (k_B), the optical transition frequency of the fundamental state of ^{133}Cs, ($\Delta\nu_{Cs}$), and the luminous efficacy of monochromatic radiation of frequency 540×10^{12} Hz, (K_{cd}). The base units (circles) deriving from such constants are respectively the ampere (A), the kilogram (kg), the meter (m), the mole (mol), the kelvin (K), the second (s) and the candela (cd). Connections between different base units are displayed by arrows.

A straightforward implication of the redefinition of the kelvin is the application of primary thermometers to a revision of the current International Temperature Scale of 1990 (ITS-90), which suffers from systematic discrepancies ranging from ppm to tens of ppm[6]. ITS-90 defines the temperature T_{90} through the combination of a certain number of fixed points of assigned temperature, such as phase transitions of pure metals, and of interpolating laws that relate the temperature between pairs of fixed points to a measurable property of a predefined thermometer, such as the electrical resistance of a standard platinum resistance thermometer. Both fixed points and interpolating laws are affected by uncertainties, which translate into departures of T_{90} values from absolute thermodynamic temperatures T. The project *Implementing the new kelvin 1* (InK1) was proposed in 2015 with the aim of fixing discrepancies between T_{90} and T in a large temperature interval[7]. Making use of primary thermometers, this initiative brought to the accurate determination of the thermodynamic temperatures of a selected set of metal-carbon mixtures and of the copper fixed point above 1358 K, as well as the temperatures of the triple point of mercury (234.3156 K), of water (273.16 K) and of the gallium melting point (302.9146 K) in a lower temperature range [7-8]. A second ongoing project, *Implementing the new kelvin 2* (InK2)[3,9], focuses on determining $T - T_{90}$ in the 1-200 K and 430-1358 K ranges and to establish novel primary thermometry approaches to minimize current systematic inconsistencies. It is in this spirit that the interest for primary thermometers has gained more and more relevance, the goal being the definition of a new highly accurate temperature scale over a very large thermodynamic interval.

1.2. Absolute primary thermometers

Primary sensors, such as primary thermometers, are of fundamental importance for the scientific community since they are absolute sensors: on the one hand they can act as master references for other secondary sensors, on the other hand they can provide the necessary accuracy for comparisons among measurements performed in different times and different laboratories. Primary thermometry methods that are considered eligible in the MeP-K project are acoustic gas thermometry, spectral-band radiometric thermometry, dielectric constant gas thermometry, refractive-index gas thermometry, Johnson noise thermometry and optical thermometry. Acoustic gas thermometers measure the speed of sound in a diluted noble gas inside an acoustic resonator and exploit its dependence on the thermal energy to retrieve the thermodynamic temperature[10]. Spectral-band radiometric thermometers measure the spectral irradiance emitted by a light source and infer the temperature from the Planck's law for thermal radiation[11]. Dielectric constant gas thermometers leverage the pressure dependence of the electric susceptibility of a monoatomic gas as described by the Clausius-Mossotti equation, which is a function of the temperature according to the gas equation of state[12]. Refractive-index gas thermometers measure the refractive index at one or more pressures to determine the gas density and extract the temperature[13]. Johnson noise thermometers derive the absolute temperature from the thermal noise fluctuations in electrical conductors[14]. Before the redefinition of the kelvin, these primary thermometers were successfully applied to the determination of the Boltzmann constant with combined uncertainties at the ppm level, and even below for acoustic gas thermometry[15-17].

In the field of primary gas thermometry, the international community of fundamental metrology early recognized the importance of developing an optical primary method to crosscheck the temperature

determinations of the other primary approaches and to quantify and correct $T - T_{90}$ discrepancies over large intervals, thereby contributing to enhance the accuracy of the ITS-90 temperature scale. Among optical methods, Doppler Broadening Thermometry (DBT) gained particular relevance since it links the thermal energy to an optical frequency, which is the physical quantity that can be measured with the highest accuracy[18-19]. The temperature is determined from the accurate measurement of the Doppler width of an absorption line of a gas at thermodynamic equilibrium. Before the paradigmatic redefinition of the kelvin in 2019, DBT has been significantly improved and refined over the past decade to measure the Boltzmann constant with an accuracy reaching the 10 ppm level, in an effort to approach the 1 ppm benchmark of acoustic gas thermometry[11] and dielectric constant gas thermometry[12].

In a first section of this paper we review the different implementations of DBT reported so far, analysing comparatively their major outcomes and limitations. In a second section we discuss and review optical methods based on the temperature dependence of line absorbance and line intensity, which have been recently proposed and developed in an effort to overcome some of the DBT weaknesses, specifically the tight dependence of the temperature on the absorption line-shape model. A concluding section of the paper gives an overview of the field and highlights the major elements of perspective for the next evolution of laser-based thermometers.

2. Doppler broadening primary thermometry

2.1. The physical principle

In a Doppler broadening regime, i.e. at pressures where the absorption profile is not dominated by collisional effects, one of the main sources of broadening of an atomic or molecular transition is the Doppler effect, which translates the velocity distribution of the absorbers at a given temperature into a distribution of frequencies at which the optical transition can take place, as sketched in Fig. 2. Through the Maxwell Boltzmann distribution of velocities one may explicit the link between the Doppler width $\Delta\nu_D$ and the thermal energy, given by the well know equation:

$$\Delta\nu_D = \frac{\nu_0}{c}\sqrt{8\ln 2\,\frac{k_B T}{M}} \qquad (1)$$

where $\Delta\nu_D$ is the full-width at half maximum (FWHM), ν_0 is the line center frequency, c the speed of light in vacuum and M the atomic or molecular mass. The value of $\Delta\nu_D$, and thus of T through Eq. 1, is determined in DBT by fitting the experimental absorption profile with a proper line-shape model.

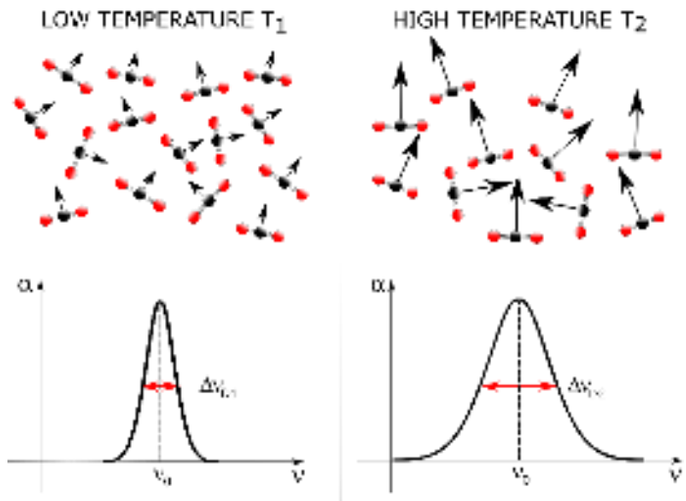

Figure 2 Graphical representation of the physical principle of DBT. At higher temperatures ($T_2 > T_1$) the thermal motion of atoms and molecules is characterized by a larger velocity distribution that determines, due to the Doppler effect, broader absorption spectral profiles (as expressed in the figure by the absorption coefficient α).

The experimental elements of major relevance for a highly precise and accurate temperature determination are (i) the selection of the transition, or transitions if multiple; (ii) the linearity and the technical noise of the detection and acquisition chain; (iii) the calibration of the optical frequency of the probe laser, which directly

impacts on $\Delta\nu_D$[20]. On the theoretical side, since the determination of T requires the fitting of an experimental absorption line, (iv) it is fundamental to adopt a proper line-shape model that fully captures all the physical mechanisms at play[20]. During the evolution of DBT, the different realizations have progressively shown the relevance of such points, which are treated in detail in the following subsections.

2.2. Sample and pressure range selection

In general, good candidates for DBT are atomic or molecular samples with a simple spectral structure and a restricted number of vibrational modes. This is indeed a favourable circumstance to have sufficiently isolated lines that can be fitted individually and to avoid line-mixing effects. The first DBT implementation[21], as well as the majority of the subsequent ones[20], focused on the accurate investigation of a single preselected transition. This approach allows to consistently enhance the signal-to-noise ratio (SNR) of the observed transition and to obtain from the residuals of the fitting an insight into the adequacy of the line-shape model adopted. On the other hand, correlations between free parameters of the fitting, such as collisional and Doppler width, may impair the accuracy of the final T determination. In this respect, probing multiple lines is a viable way to reduce correlations between these parameters, by adding, for instance, the constraint of a linear dependence of the Doppler width $\Delta\nu_D$ on the optical frequency ν_0, as established by Eq. 1[22-24]. Other elements of relevance for the choice of the transition are the absence of a hyperfine structure, which may complicate the line-shape modelling, and the sensitivity of the transition to electric and magnetic fields, which would require proper shielding of the gas container.

The range of pressure is another crucial parameter, which is related to the choice of the transition, to the sensitivity of the spectrometer, and to the line-shape modelling. In fact, the physics of self-colliding atomic or molecular gases at the origin of absorption profiles is too complex to be described analytically, which makes it relevant to select pressures where simplified line-shape profiles may be adopted without substantial accuracy penalty. DBT determinations are typically performed in a pressure range where the Doppler broadening is the dominant effect with respect to other broadening mechanisms such as the collisional broadening. In this regard, a relevant parameter is the ratio between the Doppler width $\Delta\nu_D$ and the collisional broadening $\Delta\nu_C$ (here referred to as $\delta = {}^{\Delta\nu_D}/_{\Delta\nu_C}$), with $\Delta\nu_C$ accessible from databases such as HITRAN[25] through the pressure broadening coefficients of the selected transition. The larger is the δ value (i.e. the smaller is the pressure), the less sophisticated is in general the line-shape model needed to describe the collisional physics, at least as long as saturation effects can be neglected. In fact, when investigating transitions with high electric dipole moments at low pressures, saturation effects come into play and determine, if not properly taken into account, a systematic contribution to the error budget. This is particularly true for cavity-enhanced techniques, because of the high intra-cavity power combined with typically small pressure values of few Pascal.

2.3. The vertical and horizontal axes

An accurate temperature determination requires a high quality for both the vertical (absorption) and horizontal (frequency) axes of the measurement. For the vertical axis, a particularly delicate point is the linearity of the detector, which is required not to distort the measured absorption profile. The visible and near-infrared ranges offer the best working conditions due to the high linearity of silicon (Si) and indium-gallium-arsenide (InGaAs) detectors, which are respectively characterized by a linearity of about 0.05% (2σ confidence interval) in the photocurrent range from 10^{-11} to 10^{-3} A[26] and of 0.08% in the range from 10^{-7} to 10^{-4} A[27]. With such levels, the systematic contribution of the detectors' nonlinearity in the error budget for DBT is kept below 5 ppm. Along with the linearity, it is also beneficial working with small incident powers (< 50 μW) to avoid local heating of the gas sample and corresponding systematic deviations in the temperature determination[20,28].

The accuracy of the horizontal axis of the measurement and thus of the frequency scale of the spectrometer directly affects the accuracy of the Doppler width and in turn of T. With typical Doppler widths of the order of few hundreds MHz, at least in the near-infrared, an accuracy target of 1 ppm corresponds to having a relative frequency scale accurate within few hundreds Hz on averaged spectra (for the absolute optical frequency, even MHz-level uncertainties can be tolerated, as these are weighted by optical frequencies of hundreds THz). This is technically possible by referencing the frequency of the probe laser either to a master laser oscillator locked to the peak of an atomic or molecular absorption line in a sub-Doppler regime, as reported for instance in[29-33], or to a self-referenced optical frequency comb[34]. In both cases the frequency stability can attain the 10^{-12} level, corresponding to hundreds of hertz, over times of minutes or even seconds. The use of combs and frequency stabilized lasers is also of major benefit for the long term stability, and thus for the chance to average

multiple spectra. As a result, the major burden on the measurement time typically comes from statistical arguments on the vertical axis. In fact, technical noise typically prevents the SNR of the experimental spectrum to be pushed beyond the 10^5-10^6 level per spectral point per second (1-2 orders of magnitude above the shot noise), which translates, with a typical number of spectral points between 100 and 1000, into times longer than tens of minutes, up to several hours.

2.4. The line-shape challenge

Since the early DBT implementations on molecular samples, where the spectrometers were capable to detect the absorption lines with high SNR, one of the major hurdles to reach the desired ppm-level accuracy was the modelling of the collisional effects, in particular the speed dependence of the relaxation rates affecting the absorption profile[20,35-36]. The basis of the line-shape theory starts from the description of the sample absorption by the well-known Beer-Lambert law, which provides the evolution of the transmitted intensity $I(\tilde{\nu})$ as a function of the wavenumber $\tilde{\nu}$ of the optical radiation (expressed in cm^{-1}) through the equation:

$$I(\tilde{\nu}) = I_0\, exp[-nSLg(\tilde{\nu} - \tilde{\nu}_0)] \qquad (2)$$

where $\tilde{\nu}_0$ is the line centre wavenumber of the transition (cm^{-1}), I_0 is the incident intensity (W cm^{-2}), n the gas density (molecules cm^{-3}), S the line-strength (cm molecules^{-1}), L the absorption interaction length (cm) and $g(\tilde{\nu} - \tilde{\nu}_0)$ is the line-shape function (cm) normalized to 1, namely $\int g(\tilde{\nu} - \tilde{\nu}_0)d\tilde{\nu} = 1$. The function $g(\tilde{\nu} - \tilde{\nu}_0)$ accounts for the physical processes responsible for the broadening of the transition with respect to an ideal delta-like function centred at $\tilde{\nu}_0$.

Whenever the natural broadening caused by the finite lifetime of the upper state can be neglected, which is the case for molecular substances observed in the near and mid-infrared, the broadening of a spectral line is determined by two main processes: (i) the thermal motion of the atoms or molecules described by a Gaussian profile through the Maxwell-Boltzmann function and (ii) the binary collisions between them causing a Lorentzian profile. If these processes can be considered as statistically independent, a first approximation for $g(\tilde{\nu} - \tilde{\nu}_0)$ is the Voigt profile, namely the convolution of the Lorentzian and Gaussian profiles. The Voigt profile was used since the early DBT measurements, but it does not include any correlation between thermal motion and collisions. Moreover, it excludes any narrowing effect due to the speed dependence of the collisional relaxation rates and to the velocity redistribution caused by velocity-changing collisions, which are responsible for the so-called Dicke narrowing[37-38]. Figure 3 shows an example of non-Voigt effects that emerge even at pressures of few Pascal from the residuals of a fitting performed on spectra with SNR above 1000, a value that can be easily reached even without averaging.

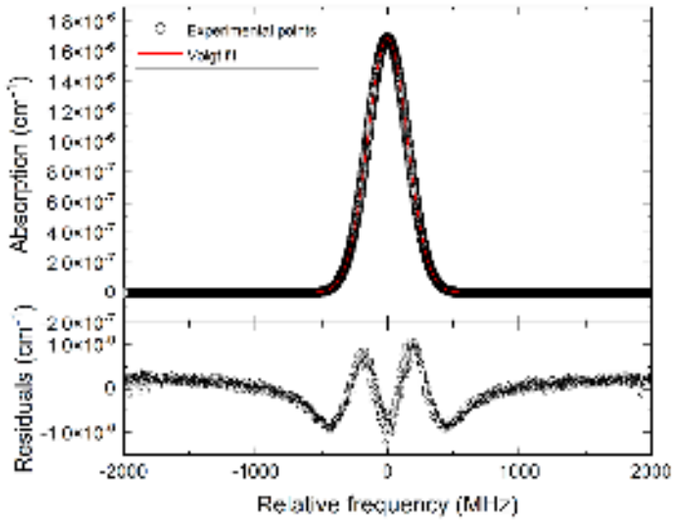

Figure 3 *CO_2 absorption spectrum of the P(12) line of the $3\nu_1+\nu_3$ band at a pressure of 7.3 Pa. The residuals from a Voigt fit clearly shows an asymmetric "w"-shaped deviation in proximity of the line center of the transition due to the combination of speed dependent effects, which are responsible for the asymmetry, and Dicke narrowing.*

In the literature, profiles including the effect of the Dicke narrowing have been developed under either the soft or hard collision approximation between the absorbing and the perturbing species. In the soft collision approximation, the velocity change induced by single collisions is negligible, thus several collisions are required to impact significantly on the velocity distribution. In this regime the absorber motion is treated as diffusive and the profile describing the absorption is the Galatry profile (GP)[39]. Differently, in the hard collision approximation each collision completely randomizes the velocity, making the new velocity conform to a Maxwellian distribution. This approximation leads to the Nelkin-Ghatak profile (HCP)[40]. As anticipated, velocity-changing collisions (Dicke effect) are not the only narrowing mechanism at play, as this would imply unrealistic values of the velocity changing collision frequency, as shown for instance in Ref.[41]. A second contribution comes from the speed dependence of the relaxation rates, which may be taken into account in the speed dependent versions of the previous profiles, namely the speed dependent GP (SDGP) and the speed dependent HCP (SDHCP)[42-43]. Both profiles treat velocity changing and speed dependent effects as statistically independent, but this is an approximation that fails to describe the line-shape beyond a certain level of accuracy, also depending on the gas pressure[44]. When a correlation is introduced together with a quadratic approximation for the speed dependence, the so-called partially correlated quadratic speed-dependent hard-collision profile (pCqSDHCP), commonly referred to as Hartmann-Tran profile (HTP)[45], is found. HTP has been recently accepted by the spectroscopic community as the new paradigm to describe absorption line-shapes beyond the Voigt profile.

Under the quadratic approximation for the collisional width Γ and shift Δ, which are initial assumptions for HTP, the complex dephasing collision frequency $\Gamma + i\Delta$ is expressed as a function of the square of the atomic or molecular speed v according to the formula:

$$\Gamma(\boldsymbol{v}) + i\Delta(\boldsymbol{v}) = (\Gamma_0 + i\Delta_0) + (\Gamma_2 + i\Delta_2) \times \left[\left(\frac{v}{\hat{v}}\right)^2 - \frac{3}{2}\right] \quad (3)$$

where $\hat{v} = \sqrt{\frac{2k_B T}{m}}$ is the most probable speed of the molecules, Γ_0 and Δ_0 are the collisional width and shift averaged over all molecular speeds, Γ_2 and Δ_2 are the quadratic contributions. The latter are linearly related to Γ_0 and Δ_0 by $\Gamma_2 = a_w\Gamma_0$ and $\Delta_2 = a_s\Delta_0$, with a_W and a_S depending on the specific intermolecular potential[46]. In this approximation, apart from normalization constants, the HTP expressed as a function of $\tilde{\nu}$ takes the form:

$$g(\tilde{\nu} - \tilde{\nu}_0) \propto Re\left\{\frac{A(\tilde{\nu}-\tilde{\nu}_0)}{1-\left[\beta-\eta\left(C_0-\frac{3C_2}{2}\right)\right]A(\tilde{\nu}-\tilde{\nu}_0)+\left(\frac{\eta C_2}{\hat{\nu}^2}\right)B(\tilde{\nu}-\tilde{\nu}_0)}\right\} \quad (4)$$

where β is the frequency of velocity-changing collisions quantifying the impact of Dicke narrowing, η is the temporal correlation between velocity-changing and dipole-dephasing collisions, the terms C_0 and C_2 are respectively equal to $\Gamma_0 + i\Delta_0$ and $\Gamma_2 + i\Delta_2$, while $A(\tilde{\nu} - \tilde{\nu}_0)$ and $B(\tilde{\nu} - \tilde{\nu}_0)$ are given by the integrals:

$$A(\tilde{\nu} - \tilde{\nu}_0) = \int \frac{f_{MB}(\boldsymbol{v})}{i2\pi c\left(\tilde{\nu}-\tilde{\nu}_0-\frac{\boldsymbol{k}}{2\pi}.\frac{\boldsymbol{v}}{c}\right)+(1-\eta)\left\{C_0+C_2\left[\left(\frac{v}{\hat{v}}\right)^2-\frac{3}{2}\right]\right\}+\beta} d\boldsymbol{v} \quad (5)$$

$$B(\tilde{\nu} - \tilde{\nu}_0) = \int \frac{v^2 f_{MB}(\boldsymbol{v})}{i2\pi c\left(\tilde{\nu}-\tilde{\nu}_0-\frac{\boldsymbol{k}}{2\pi}.\frac{\boldsymbol{v}}{c}\right)+(1-\eta)\left\{C_0+C_2\left[\left(\frac{v}{\hat{v}}\right)^2-\frac{3}{2}\right]\right\}+\beta} d\boldsymbol{v} \quad (6)$$

being $f_{MB}(\mathbf{v})$ the Maxwell-Boltzmann distribution and $k = {}^{2\pi}/_{\lambda}$ the wavenumber. Thanks to the implementation provided by Ngo *et. al* in Ref.[47], the HTP can be efficiently integrated into a fitting routine requiring a small computation effort. Moreover, it is particularly versatile because it can describe simpler profiles by fixing to zero some of its parameters[45]. Typically, if the quality of the spectra analysis does not improve by leaving as free parameters β and η, these are fixed to zero, meaning that in the selected pressure range the speed-dependent version of the Voigt profile (SDVP) is a good model of the absorption line-shape. Historically, before the HTP recommendation, the SDVP was indeed among the preferred models.

Depending on the working pressure or on the selected thermometric substance, even HTP may not match a given accuracy target, mostly due to an inaccurate description of the correlation between velocity-changing and rotational-state changing collisions. More sophisticated profiles may better account for the hardness and duration of collisions, for instance the partially correlated speed-dependent Keilson-Storer (PCSDKS) model

[48], but due to their complexity they cannot be implemented into fitting routines. A viable solution that has been pursued in Ref.[68] is to include an hypergeometric modeling of collisional and shifting effects [31], overcoming the quadratic approximation used in HTP. The discussion of profiles beyond HTP is however left to more specific papers [48-50]. It is simply reminded here that a profile of increased complexity is typically accompanied by a higher number of descriptive parameters and that handling their physical and numerical correlation, for example between the Dicke narrowing and the narrowing caused by the speed-dependent broadening, may be far from trivial. To partially remove correlations between parameters and favor the convergence of the fitting towards physically significant spectroscopic parameters, a multispectrum fitting procedure of the experimental data acquired at different pressures is usually adopted [51-52]. A global fitting procedure is an extension of the nonlinear least square spectrum fitting to account simultaneously for multiple spectra. This approach reduces the overall number of fitted parameters as compared to an independent fitting of each spectrum, as it introduces scaling laws between spectroscopic and thermodynamic parameters in conformity with the physics of the problem, such as the linear dependence of the collisional broadening on pressure or the independence of the Doppler width on pressure. When using complex profiles with a high number of descriptive parameters, the robustness of the fitting and the physical meaning of the fitting results can be further enhanced by *ab-initio* calculation of certain parameters[53], but these advancements have not impacted primary thermometry yet.

3. High precision and accuracy laser-based thermometers

The history of laser-based primary thermometry starts with the proposal of Bordé in 2005[18] where it was suggested to exploit the link between the thermal energy of the gas sample and the Doppler width to determine the Boltzmann constant[18-19]. This was also the origin of DBT. After this proposal, several research groups implemented optical systems targeting different samples of both atomic and molecular nature, with transitions from the visible to the mid infrared, developing several procedures to analyze the experimental data. Figure 4 reports the evolution across the years of the accuracy of these optical systems, from above 100 ppm for the first implementations down to around 10 ppm for the best DBT demonstrations. This was not sufficient for DBT to constraint the CODATA value for k_{B} introduced in 2019, which was given with an uncertainty of about 1 ppm on the basis of other primary approaches[1]. However, DBT is likely to play a decisive role in the new scenario followed by the redefinition of the kelvin, for instance to solve inconsitencies of the ITS-90 scale that range from few ppm, or even below around the TPW, to tens of ppm[7,54]. In a future perspective, as described later in this review, research is also ongoing on improving DBT and make it competitive with the current benchmark of acoustic and dielectric constant gas thermometry. In the next section we describe and comparatively analyze with some detail the thermometers that populate Fig. 4, including both those relying on DBT and those recently reported based on the line absorbance or line intensity temperature dependence. The accuracy of the latter methods is currently at the level of 100-1000 ppm, but thanks to a rapid evolution also prompted by recent technical advancements, they have a great potential for fast and accurate temperature measurements in industrial, scientific or metrological domains, most of all where high pressures and temperatures are used, and where the fitting of individual lines followed by DBT analysis might be hampered by the presence of multiple overlapping lines.

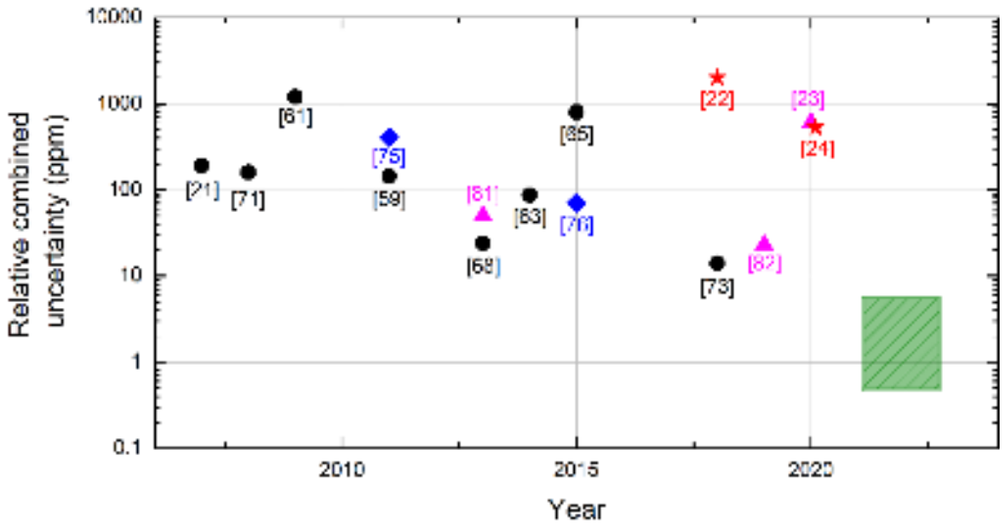

Figure 4 Combined uncertainties of laser-based thermometry approaches reported so far over time with corresponding reference numbers: single-transition DBT on molecular samples (black dots), DBT on atomic samples (blue diamonds), multi-transition DBT (pink triangles), line absorbance or line intensity based thermometry (red stars). The shaded green rectangle indicates the expected level of combined uncertainty of ongoing projects.

3.1. Single-transition DBT

3.1.1. Molecular targets

The first DBT implementation was on a molecular transition of ammonia (NH_3) at 10.35 µm measured by Daussy *et al.* in 2007[21]. NH_3 has a pyramidal structure with three identical N-H bonds leading to four vibrational modes. Due to the nuclear spins of N and H, hyperfine structure effects must be considered in the spectral analysis. The choice of ammonia was motivated by the fact that the sQ63 transition in the ν_2 band around 10 µm is characterized by a line-strength of 10^{-20} cm/molecules that provides a significant absorption signal even in a relatively short cell (37 cm) at low pressures. It is also relatively stronger than neighbouring lines and is sufficiently isolated to be studied neglecting line-mixing effects. Using as a probe laser the sideband of a 10 Hz-linewidth frequency-stabilized CO_2 laser, the sQ(63) transition profile was acquired in the pressure range 1-10 Pa with the gas housed in a thermalized cell at 273.15 K. The analysis of 2000 spectra with a Gaussian profile provided a combined uncertainty of 190 ppm in the determination of the Boltzmann constant, mostly due to the basic Gaussian line profile adopted for the fitting of spectra (which resulted in an unrealistic linear dependence of the Doppler width on pressure) and to parasitic light reaching the detector. Few years later, the same group improved the line-shape analysis adopting the Voigt profile first, SDVP after [55-56]. Moreover, the setup was upgraded with the use of a multi-pass cell, making it capable to investigate the selected transition in the pressure range 0.1-2.5 Pa and with an improved thermal stabilization [57]. The analysis of 7171 spectra provided a statistical uncertainty of 6.4 ppm and a combined uncertainty of 144 ppm[58-60]. After the first demonstration on ammonia, DBT moved towards simpler molecular samples characterized by suitable transitions in the near-infrared region (0.7-2 µm range), which is favourable for the linearity of the detectors. Among such samples, acetylene (C_2H_2), water (H_2O) and carbon dioxide (CO_2) represented the molecular targets of election.

Acetylene is a linear molecule with five vibration modes and no permanent dipole moment, which strongly reduces the interactions with the walls of the gas container. Despite its relatively large number of vibration modes, it is possible to find strong and well isolated transitions around 1.54 µm in the well-known $\nu_1+\nu_3$ absorption band. In 2008, Yamada *et al*. performed DBT measuring the direct absorption spectrum of the ^{13}C acetylene line P(16) at 1.5 µm[61-62]. Using an extended cavity diode laser (ECDL) phase locked to a tooth of a self-referenced frequency comb, absorption spectra were acquired in the pressure range 40-650 Pa, each spanning 2 GHz through the tuning of the comb repetition rate. With an analysis restricted to 20 acquisitions and the adoption of a Voigt profile, the accuracy on k_B determination was about 1200 ppm, mainly related to the missing temperature stabilization of the cell and to the presence of interference fringes[61-62]. Another DBT experiment based on acetylene direct absorption spectroscopy was performed in 2014 on the P(25) line of the same $\nu_1+\nu_3$ band by Hashemi *et al*.[63], using a Fabry-Perot interferometer and a wavelength meter for the

calibration of the frequency axis and SDVP for the spectral fitting. They determined the Boltzmann constant with a combined uncertainty of 87 ppm, which resulted from the quadrature addition of 86 ppm and 19 ppm statistical and systematic contributions, respectively. DBT was also applied on acetylene in 2011 by Sun *et al.*[64] and later in 2015 by Cheng *et al*. on the R(9) transition of the $\nu_1+3\nu_3$ band of acetylene at 787 nm[65]. Thanks to cavity ring-down spectroscopy, where recently local heating for DBT effects have been evaluated [28], they could operate at low pressure, down to 1.5 Pa, while maintaining a sufficiently high SNR for accurate Doppler width determinations. The probe laser frequency was calibrated through the beat-note with a reference laser locked to an ultra-low expansion (ULE) cavity through the Pound-Drever-Hall (PDH) technique. The acquisition of about 120 spectra, each one spanning about 5 GHz, led to the determination of k_B with a remarkably small statistical uncertainty of 6 ppm; on the other hand, the combined uncertainty was hampered by a systematic contribution as high as 800 ppm, dominated by the presence of weak interfering lines causing line-mixing effects[65].

Water is another good target for optical thermometry in the 0.9-1.7 μm region. Indeed, due to its smaller mass with respect to other targets used for DBT, C_2H_2 and CO_2 for instance, it is characterized by large vibrational frequencies and a larger Doppler width. Moreover, in the near-infrared, it has vibrational bands with spectral intensities at the level of 10^{-20} cm/molecule. Hyperfine structure effects are only present for the transitions of the ortho-isomer, but the line splitting is four orders of magnitude smaller than the Doppler width and thus negligible for the majority of investigations [66-67]. In 2013, Moretti et al. successfully applied DBT to the $4_{4,1}\rightarrow4_{4,0}$ line of the $H_2{}^{18}O$ $\nu_1+\nu_3$ band at 1.39 μm for an optical determination of the Boltzmann constant[68] to within a combined uncertainty of 24 ppm. The retrieved constant could be cross-checked against the CODATA value thanks to a TPW stabilization of the gas temperature[69]. The probe laser was offset-frequency locked to a reference laser stabilized on the sub-Doppler peak of a nearby $H_2{}^{18}O$ transition to ensure repeatability and accuracy to the frequency axis. The gas sample was enclosed in a TPW-thermalized cell and probed in a pressure range from 150 to 500 Pa. A refined line-shape analysis was for the first time applied to DBT, based on the partially-correlated speed dependent hard collision profile with hypergeometric modeling of speed dependent effects (pcSDHCP) [31]. The sophistication of the profile adopted, overcoming approximations present in HTP, together with a global fitting procedure over 718 multi-pressure spectra with SNR of about 5000, positively concurred to squeeze the combined uncertainty to 24 ppm[68,70]. At the same time, it was found that the largest contribution to the error budget was due to the line-shape model itself, indicating that better determinations were needing either better models or simpler molecular targets to be modelled.

Carbon dioxide is a third excellent candidate for optical thermometry in the near-infrared. Like acetylene, it is a linear molecule with no permanent dipole moment and no hyperfine structure effects. Being centrosymmetric, it has only three fundamental modes of vibrations, thus showing a simpler spectral structure than other polyatomic molecules. The first successful DBT implementation on the R(12) line of the $\nu_1+2\nu_2+\nu_3$ of CO_2 was performed in 2008 at 2 μm by Casa *et al.*[71]. The transition was probed by an ECDL using a direct absorption cell stabilized at two different temperatures, the TPW and the gallium melting point, at a pressure of 100 Pa. The analysis of 50 spectra with a Voigt profile returned a combined uncertainty of 160 ppm in the Boltzmann constant determination[71-72]. Years later carbon dioxide at pressures of few Pascal, thus in a relatively simple collisional regime, was shown to be the right sample to overcome the 24 ppm benchmark on water. The experiments were performed by our group on the P(12) line of the $3\nu_1+\nu_3$ band of carbon dioxide at 1.578 μm[73]. Thanks to an enhancement cavity with finesse > 120000 and to a comb-locked cavity-ring-down-spectroscopy apparatus[74], absorption spectra (shown in Fig. 5a) could be acquired in a low-pressure range (1-7 Pa) at high SNR (>1000) over thousands of spectral points (> 1000) and with the further benefit of a highly accurate frequency axis dictated by the optical frequency comb. The total number of spectra acquired amounted to 35. They were processed in 7 groups of 5 spectra by global fitting routines based on the SDVP profile, returning temperatures with a peak-to-peak excursion of 20 mK (67 ppm), as shown in Fig. 5b. The error budget computation gave a combined uncertainty of 14 ppm, the smallest reported so far, resulting from the quadrature addition of 8 ppm and 11 ppm for statistical and systematic contributions, respectively. Again, the main limiting systematic term was found be the line-shape model selected for the analysis[74].

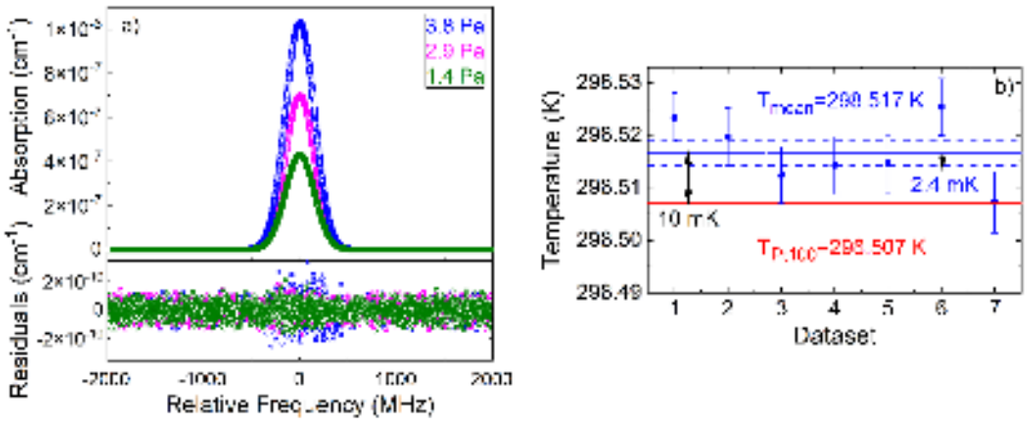

Figure 5 a) Sample spectra of the P(12) line of CO_2 at 3.8, 2.9 and 1.4 Pa analyzed in Ref.[73] with corresponding residuals from a SDVP global fit. b) Temperatures retrieved from the global fit of seven independent datasets (blue dots) together with error bars given by the statistical uncertainty at 1σ. The blue line is the mean value of all datasets, which has a statistical uncertainty of 2.4 mK (8ppm) and is in very good agreement with the temperature measured by the Pt100 sensor used to stabilize the high finesse cavity. The combined uncertainty of the mean temperature amounts to 14 ppm after quadrature addition of a systematic contribution of 11 pm.

3.1.2. Atomic targets

While molecular samples have been studied soon after the first DBT proposal, atomic samples have been the subject of DBT starting from 2011[75]. A primary advantage of a low-pressure atomic vapour system with respect to a molecular species is that atomic motion is effusive, so collisions are extremely rare, simplifying the description of collisional effects perturbing the absorption profile. Moreover, atomic transitions are also typically stronger than their corresponding molecular transitions, particularly in the visible or near-infrared region. This enables adopting very low pressures (10^{-4}-10^{-5} Pa) and neglecting collisional line-shape perturbations. Conversely, the natural linewidth cannot be neglected in the spectral analysis, together with effects such as magnetic sensitivity, hyperfine structure splitting, optical pumping and saturation effects[75-77].

Rubidium has been the first atomic target selected for high precision and accuracy optical primary thermometry, in particular the D(2) line at 780 nm probed by Truong *et al.* in 2011[75]. Due to the high intensity of the atomic transition, it was possible to use a thermally isolated 10-cm long cell at 295 K filled with a pressure of only $3 \cdot 10^{-5}$ Pa while maintaining SNRs well above 1000. The probe laser was an ECDL PDH-locked to a tuneable optical Fabry-Perot cavity whose resonant frequency was actively controlled through the beat-note with a stable Ti:sapphire laser. This reference laser was in turn locked to an ULE cavity with a frequency stability at the kHz level. The optical power in the Rb cell was 500 times below the saturation power. The acquisition of 24 spectra spanning 3 GHz and their fitting with a Voigt profile corrected for optical pumping effects returned a combined uncertainty of 410 ppm, mainly limited by residual amplitude noise in the feedback loop of the probe laser and by magnetic perturbations[75].

In 2015, the same group moved to atomic Caesium, specifically the $6S_{1/2}$-$6P_{1/2}$ hyperfine splitting of the D(1) line at 894 nm[76-77]. Using a similar spectroscopic system of that reported in Ref.[75] the gas was probed at a pressure of 10^{-5} Pa and at a temperature of 296 K inside a 7.5 cm long thermally and magnetically isolated cell. Spectral measurements over almost 7 GHz s provided a very high precision, down 6 ppm thanks to shot-noise limited detection. Conversely, the combined uncertainty was limited to 71 ppm because of saturation and laser linewidth effects that could not be properly modelled[76-77].

Within the class of atomic targets it is worth citing the ongoing DBT project on the S(0)-P(1) intercombination line of mercury at 253.5 nm proposed by L. Gianfrani and co-workers[78-80]. The accuracy of this thermometer will be soon characterized at the triple point of water, where the vapour pressure is sufficiently small to neglect any collisional broadening yet sufficiently high for the acquisition of high SNR spectra dominated by a Doppler width of about 2 GHz. In a second phase, other temperatures will be explored. The selected UV transition of Hg is more favourable for DBT with respect to those previously used with Rb and Cs because the ratio between the Doppler and the natural width is higher. A sub-kHz linewidth laser to probe the transition has been already developed in Ref.[78], together with a properly designed UV detector with a small linearity defect of about $4 \cdot 10^{-}$

^{5} for incident powers in the 50-300 nW range[79]. A temperature stability of 0.05 mK at the TPW over more than 15 hours is guaranteed by a thermostatic chamber realized to contain a non-cylindrical quartz cavity housing the mercury vapours[80]. Since the selected transition is poorly affected by nearby resonances and magnetic effects can be neglected through proper shielding, the experiment is planned to reach a final accuracy of 1 ppm in the determination of the thermodynamic temperature[78].

Table 1 summarizes in chronological order experimental conditions and achieved uncertainties for all DBT determinations above discussed, which focus on the observation and analysis of a single transition. In many cases the statistical contribution to the error budget is at the sub-10 ppm level, whereas in no case the systematic contribution is reported below 10 ppm. Therefore, the limiting factor is not the technical quality of the spectrometers, whether based on cavities or on simple cells, calibrated via master oscillators or frequency combs. Moreover, with a higher number of measurements the statistical error would be susceptible for further reductions. The bottleneck appears to be, in the best DBT demonstrations, the modelling of the line-shape profile. For molecular samples this derives from the difficulty to fully capture the physics of collisions in an analytical profile[20,73], whereas for atomic vapours the limitations are quantum interference, hyperfine splitting and saturation effects[76]. These stumbling blocks have fostered the interest towards alternative thermometry approaches that are less sensitive to the adopted line-shape model: these are the subject of the next subsection.

Year	Thermometric substance	Selected transition	Temperature (K)	Wavelength (μm)	Probe laser frequency calibration	Line-shape model	Statistical uncertainty (ppm)	Systematic uncertainty (ppm)	Combined uncertainty (ppm)	Ref.
2007	NH_3	sQ(63)	273.15	10.35	Electro-optic tuning of an OsO_4-dip-stabilized CO_2 laser	Gaussian	--	--	190	[21]
2008	CO_2	R(12)	270 - 330	2	High finesse resonator + etalon	Voigt	--	--	160	[71]
2008	C_2H_2	P(16)	294.65	1.54	Phase locking to a comb tooth	Voigt	--	--	1200	[61]
2011	NH_3	sQ(63)	273.15	10.35	Electro-optic tuning of an OsO_4-dip-stabilized CO_2 laser	Voigt	7	143	144	[59]
2011	Rb	D(2)	≈295	0.78	Beat-note signal with a ULE-stabilized reference oscillator	Voigt corrected for optical pumping effects	397	102	410	[75]
2013	H_2O	$4_{4,1}\rightarrow4_{4,0}$	TPW	1.39	Offset-frequency locking to an $^{18}H_2O$ dip-stabilized reference oscillator	pcSDHCP with hypergeometric modelling of collisional and shifting effects	16	18	24	[68]
2014	C_2H_2	P(25)	295.78	1.54	Wavelength meter + Fabry-Perot interferometer	SDVP	86	19	87	[63]
2015	Cs	D(1)	≈296	0.89	Offset-frequency locking to a master laser stabilized	Voigt corrected for optical pumping effects	6	70	71	[76]

					to the D(1) transition of Cs					
2015	C_2H_2	R(9)	299 - 306	0.78	Beat-note signal with a ULE-stabilized reference oscillator	Rautian	12	799	800	[65]
2018	CO_2	P(12)	298.52	1.58	Frequency locking to a comb tooth	SDVP	8	11	14	[73]

Table 1 Comparative table of single-transition DBT experiments performed so far, in chronological order. From left to right the columns respectively report year of publication, thermometric substance, temperature value specifying if it conforms to ITS-90 fixed points, selected transition, wavelength, probe laser frequency calibration procedure, line-shape model employed for the fitting, statistical, systematic and combined uncertainty (1σ values expressed in ppm), and reference number.

3.2. Multiple-transitions and line absorbance thermometers

3.2.1. Multiple transition DBT

To overcome the limitation on the accuracy of DBT imposed by the line-shape analysis, one might impose additional constraints to the free parameters in the fitting routine to determine the best approximated absorption profile. In this respect, a viable way is to investigate with the same spectrometer more than one absorption line at the same thermodynamic conditions. This allows, for instance, to force a linear scaling of the Doppler width against the line centre frequency in a global fitting routine. This is beneficial to reduce the correlation in the fit between Doppler and collisional broadening and in general to make the temperature determination less sensitive or less dependent on effects perturbing a single transition.

A first attempt to apply the typical DBT approach on a triplet of transitions of the ν_2 band of ammonia around 9 µm was demonstrated by Gatti *et al.* in 2013[81]. A room-temperature continuous-wave quantum cascade laser was coherently phase locked to a thulium optical frequency comb via sum frequency generation in an $AgGaSe_2$ crystal. Frequency scans over 1 GHz were achieved by tuning the repetition rate of the comb, a span sufficiently large to acquire simultaneously the absorption profiles of the sR(6,2), sR(6,6), and sR(6,1) NH_3 lines in the 5-40 Pa pressure range at a temperature of 296 K. The analysis performed on 90 spectra resulted in a 50 ppm statistical uncertainty, with a reduction by 20 % of the correlation between Doppler and collisional width when moving from an unconstrained to a constrained case. Among the profiles tested for the analysis, SDVP resulted the most adequate, as it was the only providing a zero slope between retrieved temperature and integrated absorbance[81]. Systematic error sources were not investigated.

In 2019, Castrillo *et al.* used a comb-referenced dual laser spectrometer similar to that described above for the water experiment [68] to target a line doublet of acetylene at 1.39 µm, specifically the R(15) and P(17) lines of the $\nu_2+\nu_3+\nu_5$ and $2\nu_2+\nu_4+\nu_5$ bands, respectively[82]. The doublet spacing is sufficiently small to resolve the two transitions separately with a frequency span of only 5 GHz. On the other hand, in the investigated pressure range (60-1100 Pa), the collisional widths of the two lines were more than two orders of magnitude smaller than their relative separation, which removed line-mixing issues. The two lines were treated independently regarding collisional width and shift in a global fitting procedure based on HTP, while sharing the same thermal energy $k_B T$. With this constraint, the spectral analysis of 1180 acquisitions provided a combined uncertainty as low as 23 and 24 ppm at the TPW and at the triple point of Gallium (303 K) , respectively[82].

More recently, in 2020, Galzerano performed DBT experiments with a direct comb spectroscopy approach that enabled the simultaneous acquisition of 28 lines of the P branch of the $\nu_1+\nu_3$ band of acetylene around 1.54 µm[23]. A self-referenced Er:fiber frequency comb was coupled inside a 32m path length multi-pass cell passively stabilized at room temperature and containing C_2H_2 at pressures ranging from 10 to 100 Pa. The transmitted light was coupled to a scanning micro-cavity resonator that could accurately resolve the comb modes and reconstruct the frequency axis[83]. The individual fitting of the 28 transitions with a Voigt profile to extract the Doppler widths, together with their linear interpolation over frequency, led to the retrieval of the gas temperature with a combined uncertainty of 630 ppm even with a relatively small SNR, from 10 to 700 depending on the line[23].

3.2.2. Rotational states Distribution Thermometry (RDT) and Multispectrum-RDT (MRDT)

This class of thermometers leverages the temperature dependence of the line intensity. The intensity of an absorption transition varies as a function of the thermodynamic temperature: this experimental evidence derives from the quantum temperature dependence of the atomic or molecular polarization[84]. Considering an optical transition from a lower state, with rotational quantum number J, at a frequency ν_m (where m is equal to $J+1$ for the R-branch and $-J$ for the P-branch), the line intensity S_m can be expressed by the relation[25]:

$$S_m = I_a \times \frac{A_m}{8\pi c \nu_m^2} \times \frac{g' exp(-c_2 E''/T)[1-exp(-c_2 \nu_m/T)]}{Q(T)} \quad (7)$$

where I_a is the natural isotopic abundance on Earth, A_m is the Einstein coefficient of the transition, g' the statistical weight of the upper state, c_2 is the second radiation constant, E'' is the lower state energy and $Q(T)$ is the total internal partition sum. When dealing with optical transitions, the term in square brackets becomes negligible so that a simplified form of Eq. 7 can be used:

$$S_m \simeq I_a \times \frac{A_m}{8\pi c \nu_m^2} \times \frac{g' exp(-c_2 E''/T)}{Q(T)} \quad (8).$$

Equation 8 describes the dependence of S_m on temperature, which can be exploited, in a reversed way, to infer the temperature of the gas once S_m are measured at a given T for different m values, i.e. for different transitions. Actually, S_m terms cannot be directly measured, but they can be readily determined from the measurement of the integrated absorbances, which is why this class of thermometers is referred to as line intensity or line absorbance methods. They require measurements over several transitions, possibly over an entire rovibrational band to leverage the temperature dependence of S_m across the band. The proportionality constant between S_m and the line absorbance, given by the product of the gas number density n times the gas-radiation interaction length L, is not accessible with metrological quality, yet this barely affects the error budget since n and L do not depend on m. The very observables of these thermometric approaches are indeed the integrated and sometimes the line centre absorbances as a function of m.

An example of this kind of thermometry, denominated Rotational states Distribution Thermometry (RDT), was proposed in 2018 by Shimizu *et al.* . RTD is based on the retrieval of the individual line center absorbances of as many transitions as possible and on the fit of this distribution with an analytic equation for the line center absorbance derived from Eq. 8[22]. The first demonstration of RDT was provided analyzing dual-comb spectra[85] of the ν_1+ν_3 band of acetylene at the pressure of 60 Pa[22]. A promising 4-fold reduction of the statistical error on T was obtained as compared to a DBT analysis of the spectra performed similarly to the aforementioned approach by Galzerano[23]. The systematic uncertainty, however, was particularly high, about 3000 ppm, mainly limited by the choice of a Gaussian profile in the fit of the individual lines and by the accuracy of the reference temperature sensor[22].

Few years later in 2020, we introduced an evolution of the RDT approach called Multispectrum Rotational states Distribution Thermometry (MRDT)[24]. MRDT relies on a global fitting routine that leverages the temperature dependence of the Doppler width and of the line-strength of a manifold of transitions of the same band acquired at different pressures. Specifically, it exploits the relation between the line-strength of the m^{th} transition at the temperature to be determined, $S_m(T)$, and a line-strength value $S_m(T_{REF})$ provided by an accurate intensity model[86-89] at a reference temperature T_{REF}:

$$S_m(T) = S_m(T_{REF}) \times \frac{Q(T_{REF})}{Q(T)} \times \frac{exp\left(\frac{-E''}{k_B T}\right)}{exp\left(\frac{-E''}{k_B T_{REF}}\right)} \frac{1-exp\left(\frac{-h\nu_m}{k_B T}\right)}{1-exp\left(\frac{-h\nu_m}{k_B T_{REF}}\right)} \quad (9).$$

The temperature determinations provided by MRDT have an error budget mainly affected by the uncertainty of the model providing $S_m(T_{REF})$, due to the fact that the other quantities in Eq. 9 are typically known with lower uncertainties. Therefore, MRDT can be applied also in a reverse way on a gas of well-known temperature as a test of a given line-strength model[24]. Figure 6 reports the results of a first MRDT demonstration on 32 transitions of the 3ν_1+ν_3 band of carbon dioxide around 1.57 µm. The measurements were performed with the cavity ring-down spectrometer described in Ref.[90], driven by a continuously tunable diode laser phase-locked to an Er:fiber comb that could be tuned over 2.7 THz with a speed of about 0.17 THz/s while maintaining a frequency accuracy at the level of 50 kHz. The spectra of the 32 transitions, acquired at five different pressures,

from about 3.5 to 14.5 Pa as shown in Fig. 6a, show an average SNR of 250. We used both DBT and MRDT to process 3 independent sets of spectra and infer the gas temperature. As displayed in Fig. 6c, the average temperatures obtained with the two methods are in agreement within their combined confidence interval, yet with an advantage by a factor of 2 for MRDT in terms of statistical uncertainty. Importantly, we found MRDT results less sensitive to the selected line-shape profile, being it either the Voigt convolution or the SDVP. In our experimental conditions we couldn't check the accuracy of MRDT better than 530 ppm, mainly due to the uncertainty of our reference temperature sensor. Interestingly, however, we could verify that the use for the fitting of two completely different intensity models for $S_m(T_{REF})$, one of theoretical origin[86] and the other of experimental origin[89], didn't change the MRDT temperature by more than 30 ppm[24]. Therefore, there is a potential for MRDT to provide accuracies at the level of few tens of ppm when employing highly accurate intensity values. In this respect, it is worth mentioning that the CO_2 band explored by MRDT was the recent subject of a very accurate spectroscopic investigation by Fleisher *et al.*[91-92]. These values could be fruitfully adopted in future MRDT investigations with CO_2 samples at TPW or in highly calibrated thermodynamic conditions to assess the final accuracy afforded by the methodology.

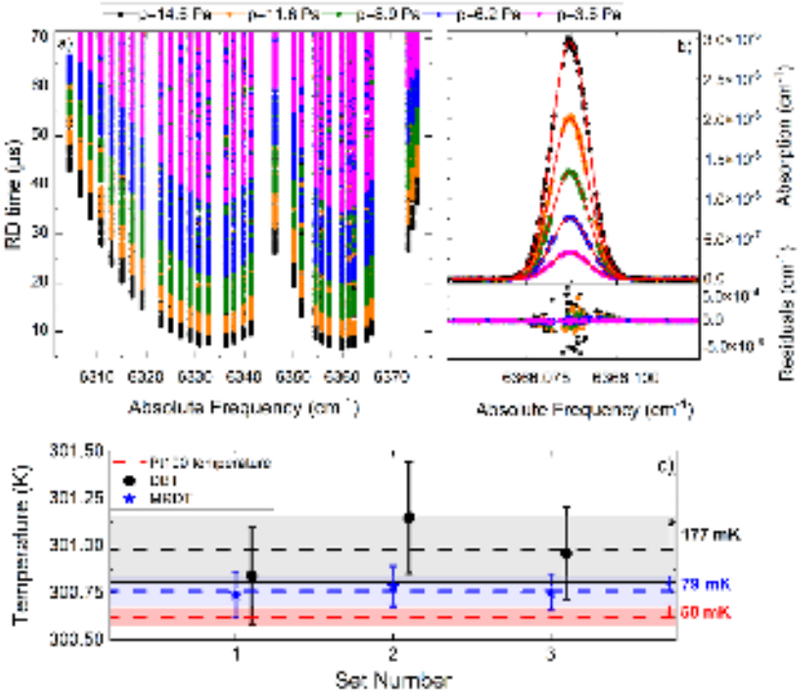

Figure 6 a) Spectra acquired at different pressures of 32 transitions of the $3\nu_1+\nu_3$ band of CO_2 (P and R branches), as measured by comb-locked frequency-swept cavity ring-down spectrometer[24,90]. b) Absorption spectra of the R26 line around 6366 cm^{-1} and residuals from SDVP fits (red curves). c) Temperatures retrieved from 3 independent datasets using MRDT (blue stars) and DBT (black dots). For DBT, the 32 individual Doppler widths were averaged together. The shaded areas correspond to the 1σ confidence interval of the mean temperature values of MRDT (blue), DBT (grey) and the reference Pt100 sensor's temperature (red)[24].

3.2.3. Line centre absorbance analysis and Line-strength Ratio Thermometry (LRT)

Besides RDT and MRDT, other two methods based on absorbance measurements have been recently proposed for optical primary thermometry: line centre absorbance analysis[82] and Line-strength Ratio Thermometry (LRT)[93]. Line centre-absorbance analysis focuses on one or multiple transitions observed at very high SNR to determine the line centre absorbance δ_0 and the integrated absorbance A at different pressures. The parameters δ_0 and A are related by the simple equation

$$\delta_0 = Ag(0) \qquad (10)$$

which may be Taylor expanded to:

$$\delta_0 = A(c_0 + c_1 A + c_2 A^2 + \cdots) \qquad (11).$$

Interestingly, the c_0 coefficient that defines the δ_0 vs A relationship at zero pressure ($A \to 0$) can be expressed as a function of the Doppler width since at decreasing pressures the absorption profile evolves into a Gaussian line-shape with $g(0) = \frac{1}{\Delta\nu_D}\sqrt{\frac{ln(2)}{\pi}}$. This enables, by simple polynomial fitting of the experimental δ_0 vs A dataset, to extract c_0 and from it the Doppler width:

$$\Delta\nu_D = \frac{\sqrt{\frac{ln(2)}{\pi}}}{c_0} \quad (12).$$

Castrillo *et al.* have tested this procedure on the acetylene line doublet that was accurately investigated with the DBT approach in Ref.[82]. They found a relevant 6-fold reduction of the statistical uncertainty with respect to DBT, but they left for the near future the investigation of systematic errors due to line-shape model adopted for the retrieval of δ_0 and A from the experimental absorption profiles.

LRT is an approach that allows to retrieve very accurately an unknown temperature T from a known temperature T_{REF}, leveraging the temperature dependence of the line-strengths S_a and S_b of two optical transitions ν_a and ν_b investigated at the two temperatures T and T_{REF}, respectively. The normalization of the ratio $R(T) = \frac{S_b(T)}{S_a(T)}$ to the ratio $R(T_{REF}) = \frac{S_b(T_{REF})}{S_a(T_{REF})}$ leads to a quantity:

$$F(T, T_{REF}) = \frac{R(T)}{R(T_{REF})} = \frac{exp\left[\frac{-h\nu_b}{k_B}\left(\frac{1}{T} - \frac{1}{T_{REF}}\right)\right]}{exp\left[\frac{-h\nu_a}{k_B}\left(\frac{1}{T} - \frac{1}{T_{REF}}\right)\right]} = exp\left[\frac{-h(\nu_b - \nu_a)}{k_B}\left(\frac{1}{T} - \frac{1}{T_{REF}}\right)\right] \quad (13)$$

which ultimately depends only on the temperature T to be determined if T_{REF} is precisely known[93-94]. The strength of the approach is that $F(T, T_{REF})$ does not depend on the partition function $Q(T)$, which is then excluded from the error budget, and can be computed by the ratio of numerically integrated absorbances, thereby circumventing also the line-shape hurdle. Although no experimental validation of LRT has been reported yet, simulations predict accuracies at the ppm level or even below for optical transitions of carbon monoxide (CO) around 4200 cm^{-1} in the temperature range 80-700 K[93-94].

Table 2 summarizes the combined uncertainties provided by multi-transition DBT and by line absorbance or line intensity methods. Apart from a combined uncertainty of 24 ppm achieved on the acetylene doublet, with an approach that closely follows that of single-transition DBT, the room for improvement is remarkable, since no other method of this class has been experimentally and theoretically developed so far till competing on equal terms with DBT or with other primary thermometry approaches. Interesting perspectives though, are opened up by recent advances in direct comb spectroscopy[95-96], with the demonstration of ultra-broadband cavity-enhanced absorption spectra measured in shot-noise limited detection conditions[97]. Cavity-enhanced direct comb spectroscopy is indeed ideally suited to probe multiple lines at high SNR and at low pressure, compensating the weakness of overtone bands with a high effective interaction length, while remaining in the near-infrared region where the frequency comb and the detector technologies are particularly mature.

Year	Thermometric substance and approach	Temperature (K)	Wavelength (μm)	Probe laser frequency calibration	Line-shape model	Statistical uncertainty (ppm)	Systematic uncertainty (ppm)	Combined uncertainty (ppm)	Ref.
2013	DBT on the sR(6,2), sR(6,6), and sR(6,1) triplet of NH_3	≈296	9	Frequency locking to a comb tooth	SDVP	50	--	--	[81]
2018	RDT on the $\nu_1+\nu_3$ band of C_2H_2	≈296	1.53	Dual comb measurement	Gaussian	≈2000	≈2000	≈3000	[22]
2019	DBT on the R(15) and P(17) doublet of C_2H_2	TPW, 302.91 (melting point of gallium)	1.39	Offset-frequency locking from a comb-referenced laser	HTP	22-23	8	23-24	[82]
2020	$\nu_1+\nu_3$ band of C_2H_2	300.1	1.54	Direct comb measurement	Voigt	633	33	630	[23]

2020	MRDT on the $3\nu_1+\nu_3$ band of CO_2	300.76	1.57	Phase locking to an endlessly tuned comb-tooth	SDVP	262	465	530	[24]

Table 2 Comparative table of multiple-transitions DBT and line absorbance/intensity thermometry experiments performed so far, in chronological order. From left to right the columns respectively report year of publication, thermometric substance and adopted approach, temperature value specifying if it conforms to ITS-90 fixed points, wavelength, probe laser frequency calibration procedure, line-shape model employed for the fitting, statistical, systematic and combined uncertainty (1σ values expressed in ppm), and reference number.

4. Conclusions and future perspectives

The interest for laser-based primary thermometry was sparked 15 years ago by the intuition to measure the elusive thermal energy of an atomic or molecular species in the gas phase through the Doppler width $\Delta\nu_D$ of an associated dipole-allowed transition, a quantity that is susceptible for being very accurately measured by the many established techniques to calibrate an optical frequency axis. The historical evolution of DBT outlined in this paper shows that a level of accuracy very close to the current state of the art (10 ppm level) was reached in a relatively short period of time, as soon as sufficiently sophisticated line-shape models together with a global fitting of multi-pressure spectra have been introduced in the retrieval of $\Delta\nu_D$. Paradoxically, line-shape models resulted afterwards the major hurdle to future reductions of the uncertainty budget, preventing DBT from competing on equal terms with other primary thermometry approaches for the determination of the Boltzmann constant, which was the preliminary step to the 2019's redefinition of the kelvin.

There are many elements that make the field extremely alive and susceptible for important advancements and applications in a near future, of both technical and fundamental nature. i) In terms of applications, the current accuracy of DBT is already sufficient to deliver primary thermometry results at the level needed to quantify and possibly reduce some uncertainties of the ITS-90 scale at temperatures far away from TPW. Therefore, it may complement the techniques and the experiments deployed in the InK2 project for the practical realization of the kelvin from the fixed value of the Boltzmann constant, providing data of high metrological quality in view of a new international temperature scale. ii) DBT is likely to take advantage in the coming years of the current effort to populate spectroscopic databases with beyond-Voigt line-shape parameters starting from ab initio quantum scattering calculations[53]. This initiative has already produced for the benchmark system of He-perturbed H_2 an entire dataset of accurate line-shape parameters (broadening and shift, their speed dependence, and the complex Dicke parameter) in a temperature from 20 to 1000 K, i.e. over most part of the ITS-90 scale. At the price of additional efforts, most of all for self-colliding molecules, *ab-initio* approaches might enrich in a next future the portfolio of accurate tools to fit absorption spectra and extract highly accurate temperature values, helping to overcome the current line-shape bottleneck. iii) Only in a relatively small number of cases has DBT been applied so far in carefully controlled thermodynamic conditions, for example at TPW or at other fixed points. For DBT to be better validated and brought to full maturity, it would be desirable to intensively apply it to thermodynamic benchmarks, even better if using different thermometric substances, different pressures and systems. iv) DBT on multiple transitions is an underexplored field that offers a unique chance to reduce the correlations that emerge in the fitting between collisional and Doppler parameters. In the frame of global fitting routines that set proper constraints to some line-shape parameters, multiple-transition DBT may effectively help reducing systematic uncertainties. v) There are many emerging spectroscopy approaches that have not been applied yet to primary thermometry and that are suited for probing multiple transitions at high temporal resolution and sensitivity without trading off the accuracy of the frequency axis[97], such as cavity-enhanced direct comb spectroscopy or the more recent frequency-swept comb-locked spectroscopy[90]. These are ideal tools for the investigation of entire rovibrational bands at low pressure, thus at high values of the ratio δ, at least in the near-infrared, which deserve new experimental endeavours. vi) The increasing availability of comb-based approaches is likely to boost also the other half of laser-based thermometers, which rely on the absorbance and line intensity distribution of multiple rotational states in a given rovibrational band. Moreover, these methods are likely to take advantage of the recent capability to measure[91] and model[92] line intensities with unprecedented accuracy by metrological calibration of the acquisition chain, which is an often neglected quantity with respect to pressure, absorber mole fraction,

temperature and so on. vii) Line absorbance and line intensity methods deserve to be further developed and applied to verify till which point they can mitigate the contribution to the temperature uncertainty from a wrong modelling of absorption line-shapes. When applied in a reverse way, i.e. using a gas of known temperature, these approaches are likely to provide a stringent testbed for the accuracy of the adopted line-strength models, fostering possible refinements of the models themselves. Better models would be of major interest, among others, for atmospheric sciences and exoplanet investigations[98-99]. viii) Experiments have been already set out to overcome the current 10 ppm accuracy barrier. One of these experiments is DBT applied to an intercombination line of Hg in the UV[78-80], which promises to break the current Cs benchmark on atomic substances, also thanks to a particularly small vapor pressure at TPW. A second experiment which should provide a 1-ppm-level accuracy with large insensitivity to line-shape issues is LRT, which is planned to be applied to two CO transitions around 4200 cm^{-1} in the 80-700 K temperature range[94].

In conclusion, an increasing number of spectroscopy approaches, technologies, applications and models, together with the realistic perspective to reach up the accuracy of other primary methods, sets solid basis to an important further evolution for laser-based primary thermometry.

Acknowledgments

The authors acknowledge a financial contribution from the project EMPATIA@Lecco ID: 2016-1428 and from the Lombardy Region Project sPATIALS3, co-funded by POR FESR 2014-2020 Call HUB Ricerca e Innovazione.

Data availability

Data sharing is not applicable to this article as no new data were created or analyzed in this study.

References

1. D.B. Newell, F. Cabiati, J. Fischer, K. Fujii, S.G. Karshenboim, H.S. Margolis, E. de Mirandés, P.J. Mohr, F. Nez, K. Pachucki, T.J. Quinn, B.N. Taylor, M. Wang, B.M. Wood, Z. Zhang, *Metrologia* **55**, L13 (2018).
2. Consultative Committee for Units (CCU) BIPM https://www.bipm.org/en/publications/si-brochure/.
3. G. Machin, J. Engert, L. Gianfrani, H. McEvoy, F. Sparasci, *Journal of Physics: Conference Series* **1065**, 122002 (2018).
4. J. Fischer, B. Fellmuth, C. Gaiser, T. Zandt, L. Pitre, F. Sparasci, M.D. Plimmer, M. de Podesta, R. Underwood, G. Sutton, G. Machin, R.M. Gavioso, D. Madonna Ripa, P.P.M. Steur, J. Qu, X.J. Feng, J. Zhang, M.R. Moldover, S.P. Benz, D.R. White, L. Gianfrani, A. Castrillo, L. Moretti, B. Darquié, E. Moufarej, C. Daussy, S. Briaudeau, O. Kozlova, L. Risegari, J.J. Segovia, M.C. Martín, D. Del Campo, *Metrologia* **55**, R1 (2018).
5. J. Fischer, *Philos. Trans. R. Soc. A-Math. Phys. Eng. Sci.* **374**, 20150038 (2016).
6. H. Preston-Thomas, *Metrologia* **27**, 3 (1990).
7. G. Machin, J. Engert, R.M. Gavioso, M. Sadli E. Woolliams, *Measurement* **94**, 149 (2016).
8. E.R. Woolliams, K. Anhalt, M. Ballico, P. Bloembergen, F. Bourson, S. Briaudeau, J. Campos, M.G. Cox, D. del Campo, W. Dong, M.R. Dury, V. Gavrilov, I. Grigoryeva, M.L. Hernanz, F. Jahan, B. Khlevnoy, V. Khromchenko, D.H. Lowe, X.Lu, G. Machin, J.M. Mantilla, M.J. Martin, H.C. McEvoy, B. Rougié, M. Sadli, S.G.R. Salim, N. Sasajima, D.R. Taubert, A.D.W. Todd, R. Van den Bossche, E. van der Ham, T. Wang, A. Whittam, B. Wilthan, D.J. Woods, J.T. Woodward, Y. Yamada, Y. Yamaguchi, H.W. Yoon, Z. Yuan, *Philos. Trans. A Math. Phys. Eng. Sci.* **374**, 20150044 (2016).
9. H.C. McEvoy, D.H. Lowe, R. Underwood, M. de Podesta, G. Machin, M.J. Martin, J.M. Mantilla, J. Campos, M. Sadli, F. Bourson, S. Briaudeau, S.G.R. Salim, K. Anhalt, M. Waehmer, D.R. Taubert, X.J. Feng, J.T. Zhang, X.F. Lu and H. Yoon, *Meas. Sci. Technol.* **32**, 035001 (2020).
10. M.R. Moldover, R.M. Gavioso, J.B. Mehl, L. Pitre, M. de Podesta, J.T. Zhang, *Metrologia* **51**, R1 (2014).
11. J. Hartmann, K. Anhalt, R.D. Taubert, J. Hollandt, *Int. J. Thermophys.* **32**, 1707 (2011).
12. C. Gaiser, T. Zandt, B. Fellmuth, *Metrologia* **52**, S217 (2015).
13. P.M. Rourke, C. Gaiser, B. Gao, D.M. Ripa, M.R. Moldover, L. Pitre, R.J. Underwood, *Metrologia* **56**, 032001 (2019).
14. J.B. Johnson, *Nature* **119**, 50 (1927).

15. L. Pitre, F. Sparasci, L. Risegari, C. Guianvarc'h, C. Martin, M.E. Himbert, M.D. Plimmer, A. Allard, B. Marty, P.A. Giuliano Albo, B. Gao, M.R. Moldover, J.B. Mehl, *Metrologia*, **54**, 856 (2017).
16. C. Gaiser, B. Fellmuth, N. Haft, A. Kuhn, B. Thiele-Krivoi, T. Zandt, J. Fischer, O. Jusko, W. Sabuga, *Metrologia* **54**, 280 (2017).
17. J. Qu, S.P. Benz, K. Coakley, H. Rogalla, W.L. Tew, R. White, K. Zhou, Z. Zhou, *Metrologia* **54**, 549 (2017).
18. C.J. Bordé, *Philos. Trans. A Math. Phys. Eng. Sci.* **363**, 2177 (2005).
19. C.J. Bordé, *C. R. Physique* **10**, 866-882 (2009).
20. L. Gianfrani, *Philos. Trans. R. Soc. A-Math. Phys. Eng. Sci.* **374**, 20150047 (2016).
21. C. Daussy, M. Guinet, A. Amy-Klein, K. Djerroud, Y. Hermier, S. Briaudeau, C.J. Bordé, C. Chardonnet, *Phys. Rev. Lett.* **98**, 250801 (2007).
22. Y. Shimizu, S. Okubo, A. Onae, K.M. Yamada and H. Inaba, *Appl. Phys. B* **124**, 1 (2018).
23. G. Galzerano, *Measurement* **164**, 107940 (2020).
24. R. Gotti, M. Lamperti, D. Gatti, S. Wójtewicz, T. Puppe, Y. Mayzlin, B. Alsaif, J. Robinson-Tait, F. Rohde, R. Wilk, P. Leisching, W.G. Kaenders, P. Laporta, M. Marangoni *New J. Phys.* **22**, 083071 (2020).
25. I.E. Gordon, L.S. Rothman, C. Hill, R.V. Kochanov, Y. Tan, P.F. Bernath, M. Birk, V. Boudon, A. Campargue, K.V. Chance, B.J. Drouin, J.-M. Flaud, R.R. Gamache, J.T. Hodges, D. Jacquemart, V.I. Perevalov, A. Perrin, K.P. Shine, M.-A.H. Smith, J. Tennyson, G.C. Toon, H. Tran, V.G. Tyuterev, A. Barbe, A.G. Császár, V.M. Devi, T. Furtenbacher, J.J. Harrison, J.-M. Hartmann, A. Jolly, T.J. Johnson, T. Karman, I. Kleiner, A.A. Kyuberis, J. Loos, O.M. Lyulin, S.T. Massie, S.N. Mikhailenko, N. Moazzen-Ahmadi, H.S.P. Müller, O.V. Naumenko, A.V. Nikitin, O.L. Polyansky, M. Rey, M. Rotger, S.W. Sharpe, K. Sung, E. Starikova, S.A. Tashkun, J. Vander Auwera, G. Wagner, J. Wilzewski, P. Wcisło, S. Yu, E.J. Zak, *J. Quant. Spectrosc. Radiat. Transf.* **203**, 3 (2017).
26. A. Thompson, H.M. Chen, *J. Res. Natl. Inst. Stand. Technol.* **99**, 751 (1994).
27. H.W. Yoon, J.J. Butler, T.C. Larason, G.P. Eppeldauer, *Metrologia* **40**, S154 (2003).
28. L. Moretti, A. Castrillo, L. Gianfrani *Phys. Rev. A* **100**, 042501 (2019).
29. N. Picqué, P. Cancio, G. Giusfredi, P. De Natale, *J. Opt. Soc. Am.* **18**, 692 (2001).
30. K. Nakagawa, Y. Sato, M. Musha, K. Ueda, *Appl. Phys. B* **80**, 479 (2005).
31. A. Castrillo, L. Moretti, E. Fasci, M.D. De Vizia, G. Casa, L. Gianfrani *J. Mol. Spectrosc*. **300**, 131 (2014).
32. G. Galzerano, E. Fasci, A. Castrillo, N. Coluccelli, L. Gianfrani, P. Laporta, *Opt. Lett.* **34**, 3107 (2009).
33. P.L.T. Sow, S. Mejri, S.K. Tokunaga, O. Lopez, A. Goncharov, B. Argence, C. Chardonnet, A. Amy-Klein, C. Daussy, B. Darquié, *Appl. Phys. Lett*. **104**, 264101 (2014).
34. D. Gatti, T. Sala, M. Marangoni, G. Galzerano, L. Gianfrani, *Enc. of Anal. Chem*. (2006).
35. A. Cygan, D. Lisak, R.S. Trawiński, R. Ciuryło, *Phys. Rev. A* **82**, 032515 (2010).
36. M.D. De Vizia, L. Moretti, A. Castrillo, E. Fasci,L. Gianfrani, *Mol. Phys.* **109**, 2291 (2011).
37. T.Q. Bui, D.A. Long, A. Cygan, V.T. Sironneau, D.W. Hogan, P.M. Rupasinghe, R. Ciuryło, D. Lisak, M. Okumura, *J. Chem. Phys.* **141**, 174301 (2014).
38. T. A. Odintsova, E. Fasci, L. Moretti, E.J. Zak, O.L. Polyansky, J. Tennyson, L. Gianfrani, A. Castrillo, *J. Chem. Phys.* **146**, 244309 (2017).
39. L. Galatry, *Phys. Rev.* **122**, 1218 (1961).
40. M. Nelkin, A. Ghatak, *Phys. Rev.* **135**, A4 (1964).
41. H. Tran, D. Bermejo, J.L. Domenech, P. Joubert, R.R. Gamache, J.M. Hartmann, *J. Quant. Spectrosc. Radiat. Transf*. **108**, 126 (2007).
42. R. Ciuryło, J. Szudy, *J. Quant. Spectrosc. Radiat. Transf.* **57**, 411 (1997).
43. B. Lance, G. Blanquet, J. Walrand, J.P. Bouanich, *J. Mol. Spectrosc.* **185**, 262 (1997).
44. N.H. Ngo, H. Tran, R.R. Gamache, J.M. Hartmann, *Phil. Trans. R. Soc. A* **370**, 2495 (2012).
45. J. Tennyson, P.F. Bernath, A. Campargue, A.G. Császár, L. Daumont, R.R. Gamache, J.T. Hodges, D. Lisak, O.V. Naumenko, L.S. Rothman, H. Tran, N.F. Zobov, J. Buldyreva, C.D. Boone, M.D. De Vizia, L. Gianfrani, J.M. Hartmann, R. McPheat, D. Weidmann, J. Murray, N.H. Ngo, O.L. Polyansky, *Pure Appl. Chem*. **86**, 1931 (2014).
46. M.D. De Vizia, A. Castrillo, E. Fasci, P. Amodio, L. Moretti, L. Gianfrani, *Phys. Rev. A* **90**, 022503 (2014).
47. H. Tran, N.H. Ngo, J.M. Hartmann, *J. Quant. Spectrosc. Radiat. Transf.* **134**, 104 (2014). Erratum to: *J. Quant. Spectrosc. Radiat. Transfer* **129**, 199 (2013).
48. N.H. Ngo, H. Tran, R. R. Gamache, *J. Chem. Phys.* **136**, 154310 (2012).

49. M. Konefał, M. Słowiński, M. Zaborowski, R. Ciuryło, D. Lisak, P. Wcisło, *J. Quant. Spectrosc. Radiat. Transfer* **242**, 106784 (2020).
50. R. Ciuryło, D. Lisak, J. Szudy, *Phys. Rev. A* **66**, 032701 (2002).
51. D.C. Benner, C.P. Rinsland, V.M. Devi, M.A.H. Smith, D. Atkins, *J. Quant. Spectrosc. Radiat. Transf.* **53**, 705 (1995).
52. A. Pasquale, M.D. De Vizia, L. Moretti, L. Gianfrani, *Phys. Rev. A* **92**, 032506 (2015).
53. P. Wcisło, F. Thibault, N. Stolarczyk, H. Jóźwiak, M. Słowiński, M. Gancewski, K. Stankiewicz, M. Konefał, S. Kassi, A. Campargue, Y. Tan, J. Wang, K. Patkowski, R. Ciuryło, D. Lisak, R. Kochanov, L.S. Rothman, I.E. Gordon, *J. Quant. Spectrosc. Radiat.* **260**, 107477 (2021).
54. R.M. Gavioso, D.M. Ripa, P.P.M. Steur, C. Gaiser, T. Zandt, B. Fellmuth, M. de Podesta, R. Underwood, G. Sutton, L. Pitre, F. Sparasci, L. Risegari, L. Gianfrani, A. Castrillo, G. Machin, *Philos. Trans. R. Soc. A-Math. Phys. Eng. Sci.* **374**, 20150046 (2016).
55. M. Guinet, C. Daussy, S. Briaudeau, A. Amy-Klein, Y. Hermier, C.J. Bordé, G. Chardonnet, *J. Phys. IV* **135**, 181 (2006).
56. F. Rohart, S. Mejri, P.L.T. Sow, S.K. Tokunaga, C. Chardonnet, B. Darquié, H. Dinesan, E. Fasci, A. Castrillo, L. Gianfrani, C. Daussy, *Phys. Rev. A* **90**, 042506 (2014).
57. S. Mejri, P.L.T. Sow, O. Kozlova, C. Ayari, S.K. Tokunaga, C. Chardonnet, S. Briaudeau, B. Darquié, F. Rohart, C. Daussy, *Metrologia* **52**, S314 (2015).
58. M. Triki, C. Lemarchand, B. Darquié, P.L.T. Sow, V. Roncin, C. Chardonnet, C. Daussy, *Phys. Rev. A* **85**, 62510 (2012).
59. C. Lemarchand, M. Triki, B. Darquié, C.J. Bordé, C. Chardonnet, C. Daussy, *New J. Phys.* **13**, 073028 (2011).
60. C. Lemarchand, S. Mejri, P.L.T. Sow, M. Triki, S.K. Tokunaga, S. Briaudeau, C. Chardonnet, B. Darquié, C. Daussy, *Metrologia* **50**, 623 (2013).
61. K.M.T. Yamada, A. Onae, F.-L. Hong, H. Inaba, H. Matsumoto, Y. Nakajima, F. Ito, T. Shimizu, *J. Mol. Spectrosc.* **249,** 95 (2008).
62. K.M.T. Yamada, A. Onae, F.L. Hong, H. Inaba, T. Shimizu, *C. R. Physique* **10**, 907 (2009).
63. R. Hashemi, C. Povey, M. Derksen, H. Naseri, J. Garber, A. Predoi-Cross, *J. Chem. Phys.* **141**, 214201 (2014).
64. Y.R. Sun, H. Pan, C.F. Cheng, A.W. Liu, J.T. Zhang, S.M. Hu, *Opt. Express* **19**, 19993 (2011).
65. C.F. Cheng, J. Wang, Y.R. Sun, Y. Tan, P. Kang, S.M. Hu, *Metrologia* **52,** S385 (2015).
66. A. Castrillo, M.D. De Vizia, E. Fasci, T. Odintsova, L. Moretti, L. Gianfrani, *Laser Spectrosc.* 31 (2016).
67. M.D. De Vizia, T. Odintsova, L. Gianfrani, *Metrologia* **53**, 800 (2016).
68. L. Moretti, A. Castrillo, E. Fasci, M.D. De Vizia, G. Casa, G. Galzerano, A. Merlone, P. Laporta, L. Gianfrani, *Phys. Rev. Lett.* **111**, 060803 (2013).
69. A. Merlone, F. Moro, A. Castrillo, L. Gianfrani, *Int. J. Thermophys.* **31**, 1360 (2010).
70. E. Fasci, M.D. De Vizia, A. Merlone, L. Moretti; A. Castrillo, L. Gianfrani, *Metrologia* **52**, S233 (2015).
71. G. Casa, A. Castrillo, G. Galzerano, R. Wehr, A. Merlone, D. Di Serafino, P. Laporta, L. Gianfrani, *Phys. Rev. Lett.* **100**, 200801 (2008).
72. A. Castrillo, G. Casa, A. Merlone, G. Galzerano, P. Laporta, L. Gianfrani, *C. R. Physique* **10**, 894 (2009).
73. R. Gotti, L. Moretti, D. Gatti, A. Castrillo, G. Galzerano, P. Laporta, L. Gianfrani, M. Marangoni, *Phys. Rev. A* **97**, 012512 (2018).
74. R. Gotti, D. Gatti, P. Masłowski, M. Lamperti, M. Belmonte, P. Laporta, M. Marangoni, *J. Chem. Phys.* **147**, 134201 (2017).
75. G.W. Truong, E.F. May, T.M. Stace, A.N. Luiten, *Phys. Rev. A* **83**, 033805 (2011).
76. G.W. Truong, J.D. Anstie, E.F. May, T.M. Stace, A.N. Luiten, *Nat. Commun.* **6,** 8345 (2015).
77. G.W. Truong, D. Stuart, J.D. Anstie, E.F. May, T.M. Stace, A.N. Luiten, *Metrologia* **52**, S324 (2015).
78. C. Clivati, S. Gravina, A. Castrillo, G.A. Costanzo, F. Levi, L. Gianfrani., *Opt. Lett.* **45**, 3693 (2020).
79. H. Dinesan, S. Gravina, C. Clivati, A. Castrillo, F. Levi, L. Gianfrani, *Metrologia* **57**, 065001 (2020).
80. G. Lopardo, F. Bertiglia, A. Barbone, M. Bertinetti, R. Dematteis, D. Giraudi, L. Gianfrani, *Measurement* **173**, 108594 (2020).
81. D. Gatti, A.A. Mills, M.D. De Vizia, C. Mohr, I. Hartl, M. Marangoni, M. Fermann, L. Gianfrani, *Phys. Rev. A* **88**, 012514 (2013).

82. A. Castrillo, E. Fasci, H. Dinesan, S. Gravina, L. Moretti, L. Gianfrani, *Phys. Rev. Appl.* **11**, 064060 (2019).
83. A. Gambetta, M. Cassinerio, D. Gatti, P. Laporta, G. Galzerano, *Sci. Rep.* **6**, 35541 (2016).
84. K.H. Illinger, C.P. Smyth, *J. Chem. Phys*. **35**, 400 (1961).
85. I. Coddington, N. Newbury, W. Swann, *Optica* **3**, 414 (2016).
86. E. Zak, J. Tennyson, O.L. Polyansky, L. Lodi, N.F. Zobov, S.A. Tashkun, V.I. Perevalov, *J. Quant. Spectrosc. Radiat. Transfer* **177**, 31 (2016).
87. R.A. Toth, L.R. Brown, C.E. Miller, V.M. Devi, D.C. Benner, *J. Mol. Spectrosc*. **239**, 221 (2006).
88. V.M. Devi, D.C. Benner, L.R. Brown, C.E. Miller, R.A. Toth, *J. Mol. Spectrosc*. **242**, 90 (2007).
89. A. Predoi-Cross, A.V. Unni, W. Liu, I. Schofield, C. Holladay, A.R.W. McKellar, D. Hurtmans, *J. Mol. Spectrosc*. **245**, 34 (2007).
90. R. Gotti, T. Puppe, Y. Mayzlin, J. Robinson-Tait, S. Wójtewicz, D. Gatti, B. Alsaif, M. Lamperti, P. Laporta, F. Rohde, R. Wilk, P. Leisching, W.G. Kaenders, M. Marangoni, *Sci. Rep*. **10**, 1 (2020).
91. A.J. Fleisher, E.M. Adkins, Z.D. Reed, H. Yi, D.A. Long, H.M. Fleurbaey, J.T. Hodges., *Phys. Rev. Lett.* **123**, 043001 (2019).
92. D.A. Long, Z.D. Reed, A.J. Fleisher, J. Mendonca, S. Roche, J.T. Hodges, *Geophys. Res. Lett.* **47** (2020).
93. L.A. Santamaria, M.S. de Cumis, D. Dequal, G. Bianco, P.C. Pastor, *J. Phys. Chem. A* **122**, 6026 (2018).
94. L.A. Santamaria, M.S. de Cumis, G. Bianco, R. Pastore, P.C. Pastor., *New J. Phys.* **21**, 113008 (2019).
95. M.C. Stowe, M.J. Thorpe, A. Pe'er, J. Ye, J.E. Stalnaker, V. Gerginov, S.A. Diddams., *Adv. Atom. Mol. Opt. Phys.* **55**, 1 (2008).
96. N. Picqué, T.W. Hänsch, *Nat. Photonics* **13**, 146 (2019).
97. A. Foltynowicz, T. Ban, P. Masłowski, F. Adler, J. Ye, *Phys. Rev. lett.* **107**, 233002 (2011).
98. P.F. Bernath, *J. Quant. Spectrosc. Radiat. Transfer* **186**, 3 (2017).
99. J. Tennyson, S.N. Yurchenko, A.F. Al-Refaie, E.J. Barton, K.L. Chubb, P.A. Coles, S. Diamantopoulou, M.N. Gorman, C. Hill, A.Z. Lam, L. Lodi, L.K. McKemmish, Y. Na, A. Owens, O.L. Polyansky, T. Rivlin, C. Sousa-Silva, D.S. Underwood, A. Yachmenev, Emil Zak, *J. Mol. Spectrosc.* **327**, 73 (2016).

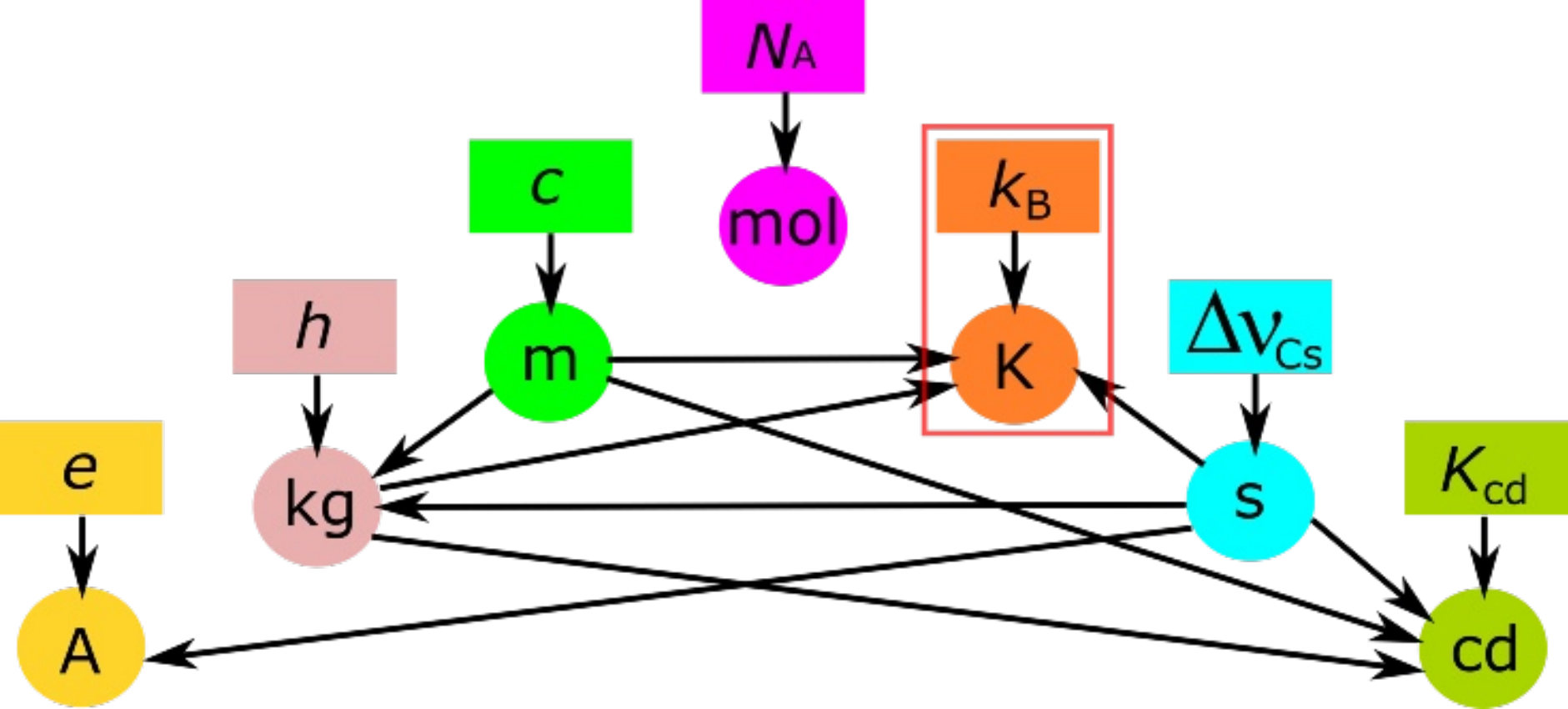
N_A
mol
c
m
k_B
K
h
kg
$\Delta\nu_{Cs}$
s
e
A
K_{cd}
cd

LOW TEMPERATURE T_1

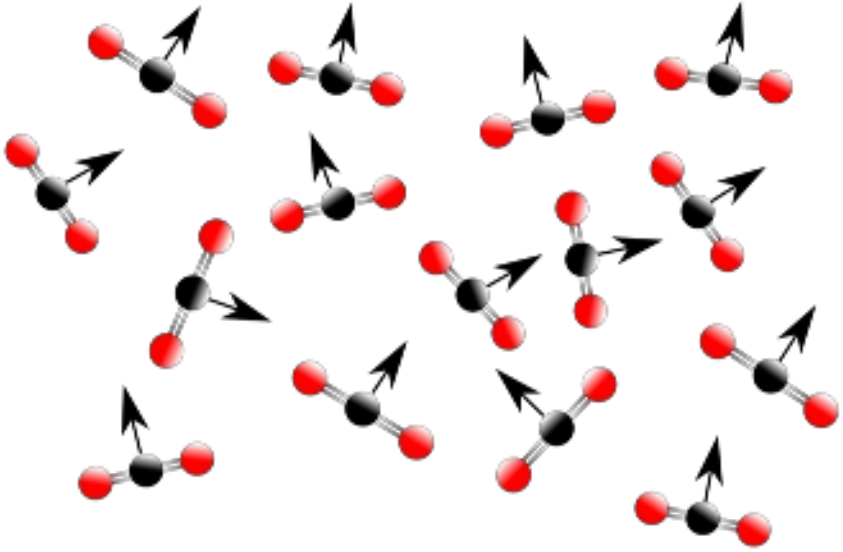

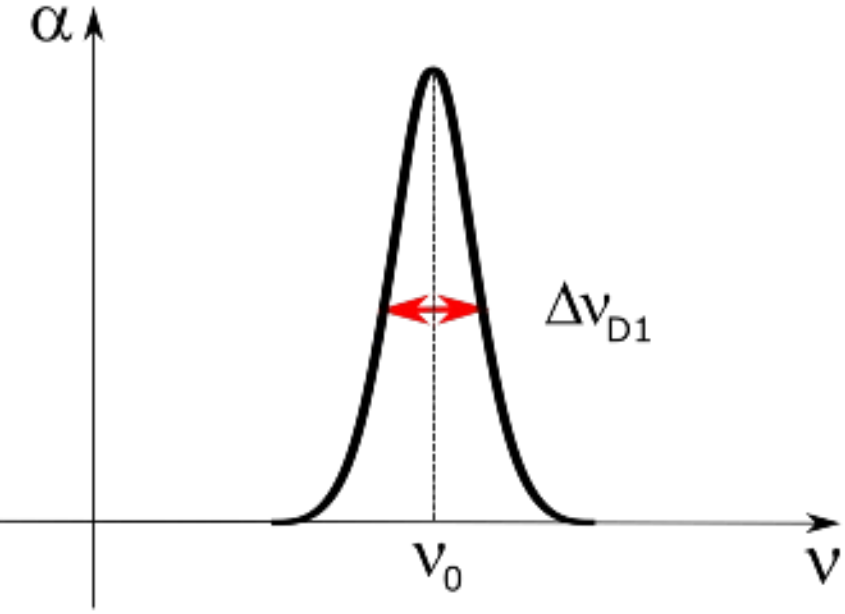

HIGH TEMPERATURE T_2

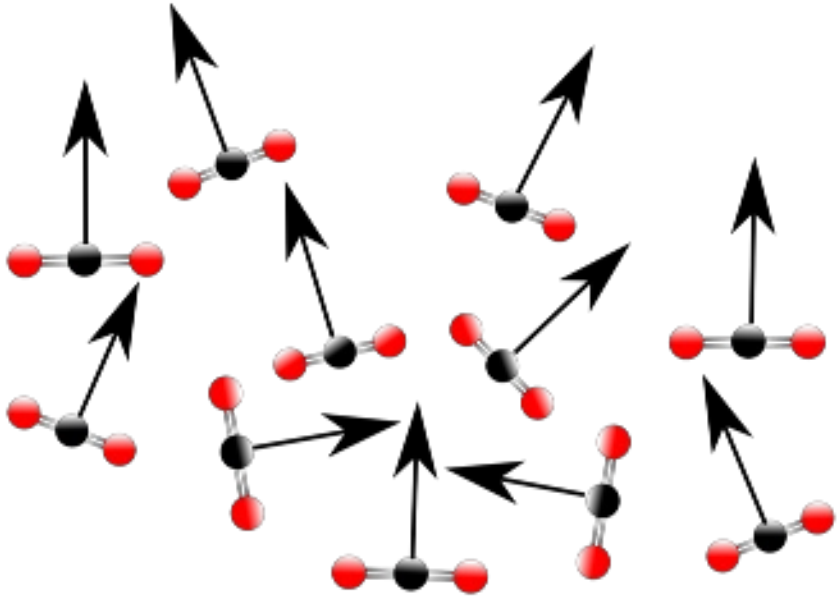

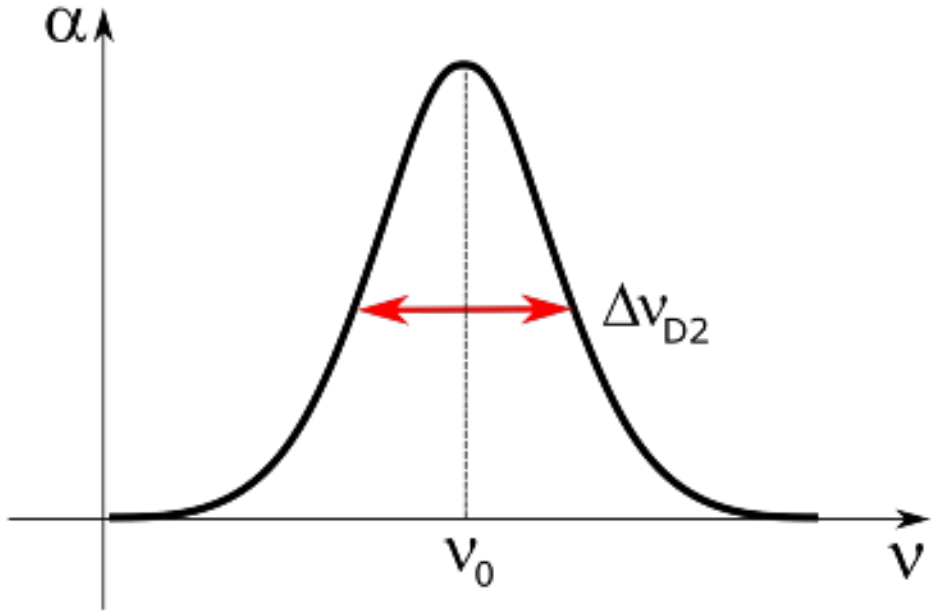

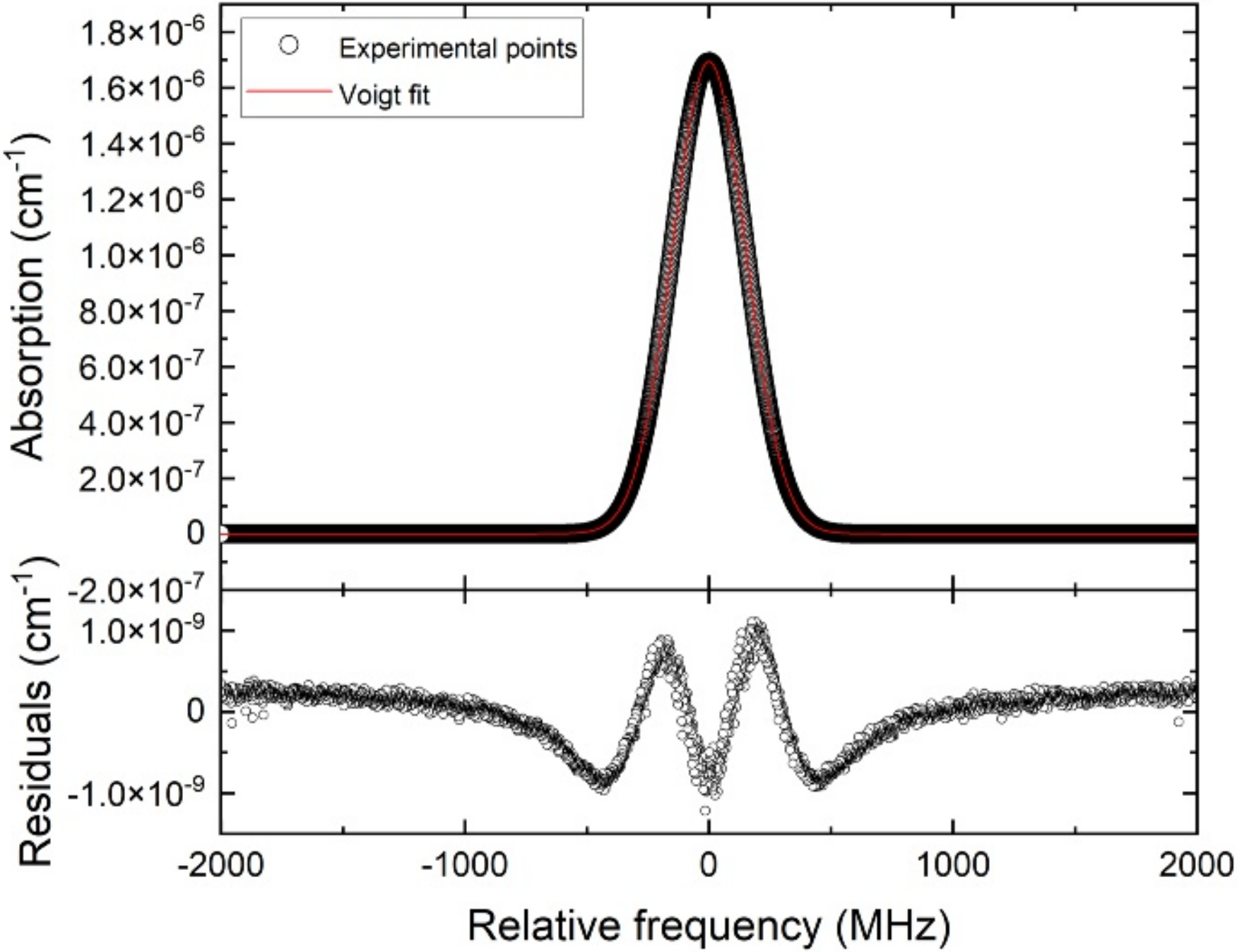
Experimental points
Voigt fit
Absorption (cm-1)
1.8×10-6
1.6×10-6
1.4×10-6
1.2×10-6
1.0×10-6
8.0×10-7
6.0×10-7
4.0×10-7
2.0×10-7
0
-2.0×10-7
Residuals (cm-1)
1.0×10-9
0
-1.0×10-9
-2000
-1000
0
1000
2000
Relative frequency (MHz)

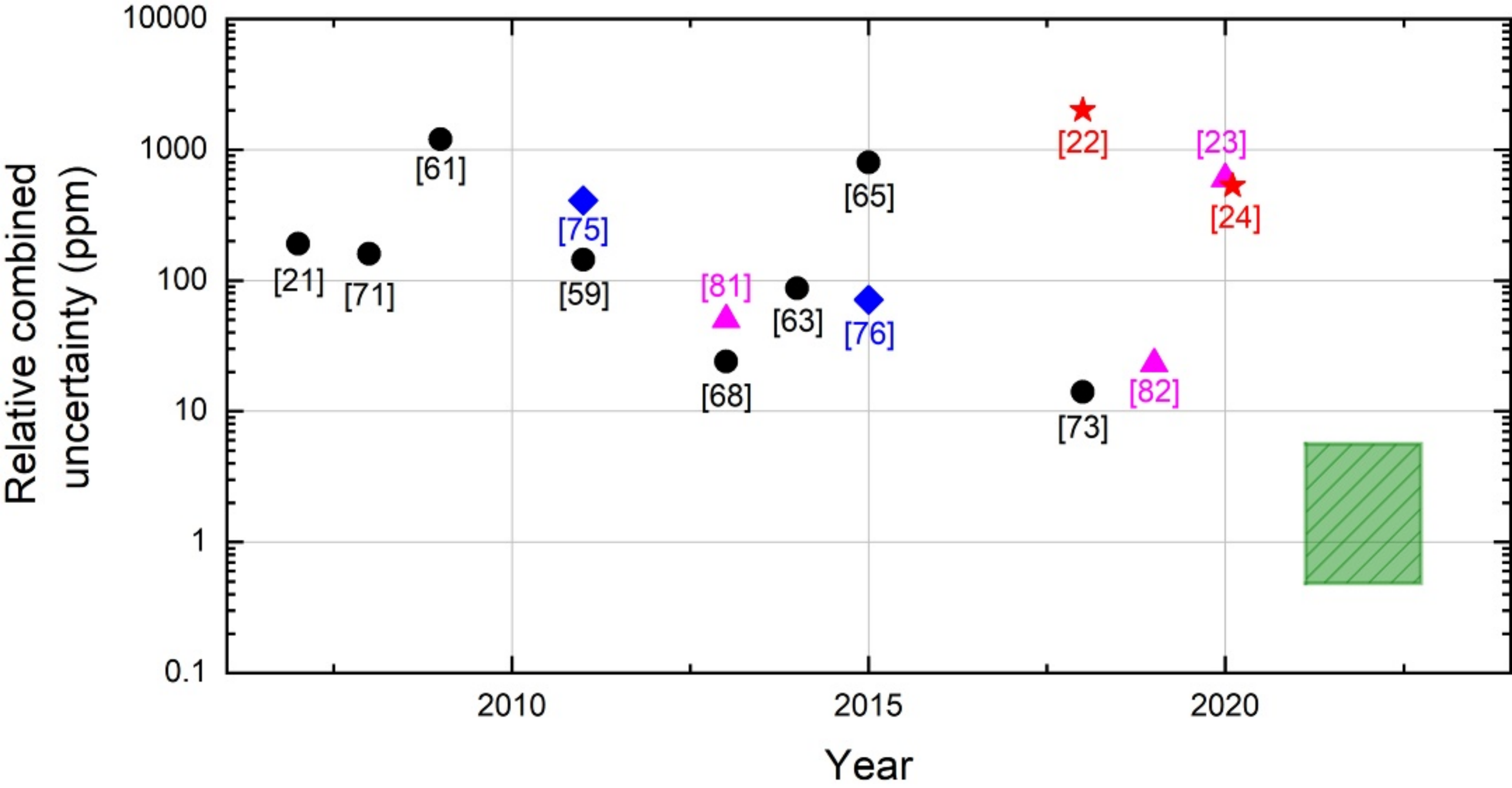
Relative combined uncertainty (ppm)
10000
1000
100
10
1
0.1
2010
2015
2020
Year
[21]
[71]
[61]
[75]
[59]
[81]
[68]
[63]
[65]
[76]
[22]
[73]
[82]
[23]
[24]

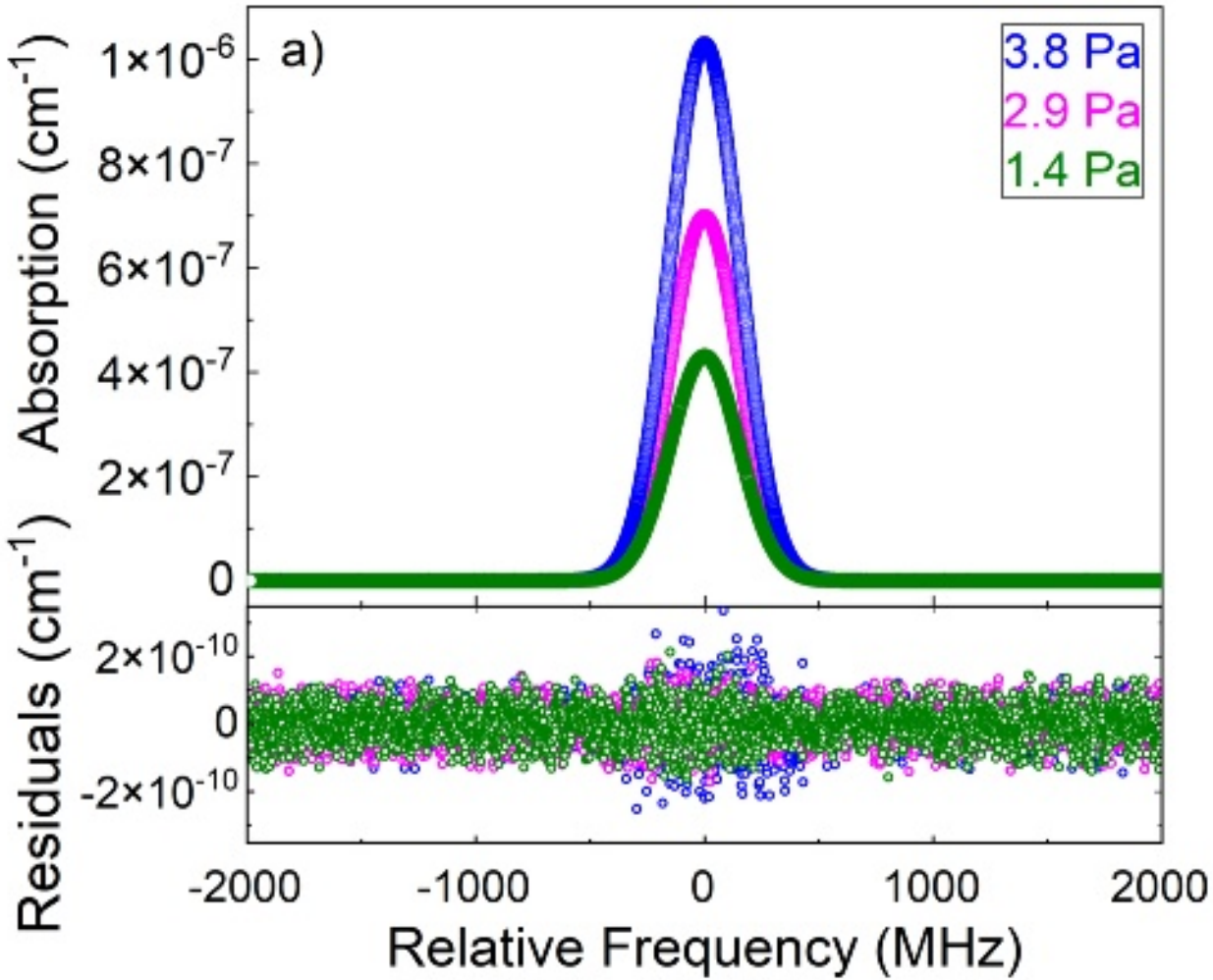
a)
3.8 Pa
2.9 Pa
1.4 Pa
Absorption (cm-1)
Residuals (cm-1)
1×10-6
8×10-7
6×10-7
4×10-7
2×10-7
0
2×10-10
0
-2×10-10
-2000
-1000
0
1000
2000
Relative Frequency (MHz)

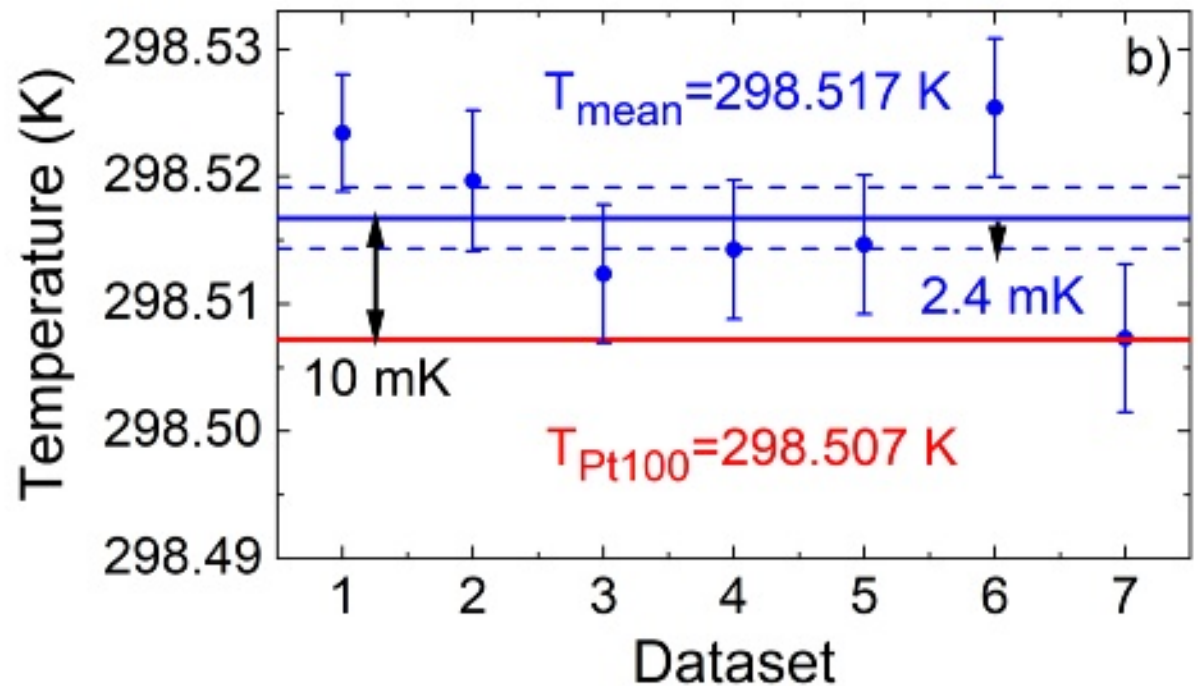
b)
Tmean=298.517 K
2.4 mK
10 mK
TPt100=298.507 K
Temperature (K)
298.53
298.52
298.51
298.50
298.49
1
2
3
4
5
6
7
Dataset

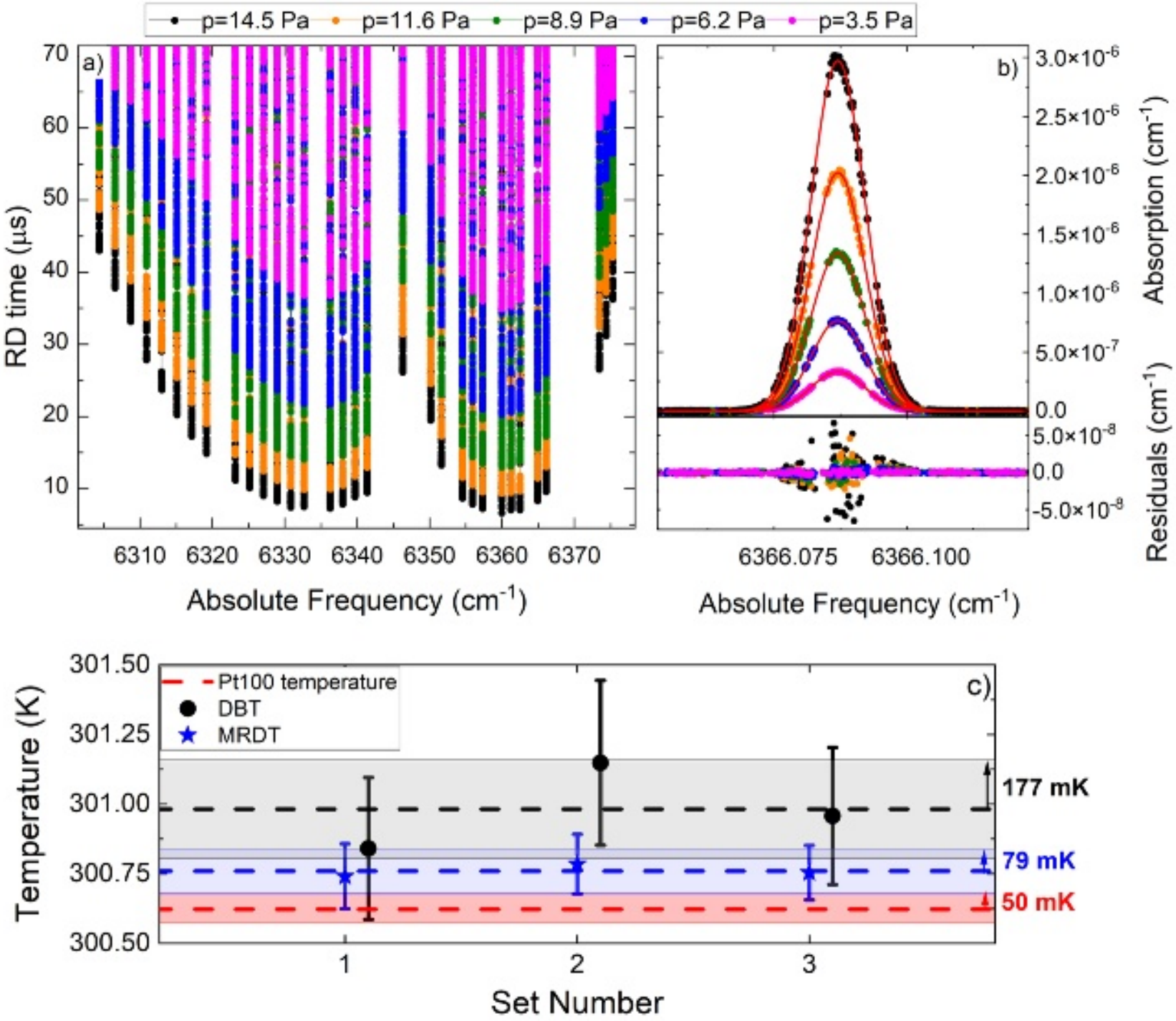
p=14.5 Pa
p=11.6 Pa
p=8.9 Pa
p=6.2 Pa
p=3.5 Pa
a)
b)
c)
RD time (μs)
Absolute Frequency (cm^{-1})
Absorption (cm^{-1})
Residuals (cm^{-1})
Temperature (K)
Set Number
Pt100 temperature
DBT
MRDT
177 mK
79 mK
50 mK